




Pseudo-time-reversal-symmetry-protected topological Bogoliubov excitations of Bose-Einstein condensates in optical lattices

Junsen Wang ,* Wei Zheng , and Youjin Deng 

Hefei National Laboratory for Physical Sciences at Microscale and Department of Modern Physics, University of Science and Technology of China, Hefei, Anhui 230026, China
and CAS Center for Excellence and Synergetic Innovation Center in Quantum Information and Quantum Physics, University of Science and Technology of China, Hefei, Anhui 230026, China



(Received 1 July 2020; accepted 28 September 2020; published 22 October 2020)

Bogoliubov excitations of Bose-Einstein condensates in optical lattices may possess band topology in analogous to topological insulators in class AII of fermions. Using the language of the Krein-space theory, this topological property is shown to be protected by a pseudo-time-reversal symmetry that is pseudo-antiunitary and squares to -1 , with the associated bulk topological invariant also being a \mathbb{Z}_2 index. We construct three equivalent expressions for it, relating to the Pfaffian, the pseudo-time-reversal polarization, and most practically the Wannier center flow, all adopted from the fermionic case, defined here with respect to the pseudo inner product. In the presence of an additional pseudo-unitary and pseudo-Hermitian inversion symmetry, a simpler expression is derived. We then study two toy models feasible on cold atom platforms to numerically confirm the bulk-boundary correspondence. The Krein-space approach developed in this work is a universal formalism to study all kinds of symmetry-protected topological bosonic Bogoliubov bands.

DOI: [10.1103/PhysRevA.102.043323](https://doi.org/10.1103/PhysRevA.102.043323)

I. INTRODUCTION

Topological band theory [1–3] is originally developed to characterize nontrivial topology of electronic bands in solids. One milestone work in the early years along this direction is the tenfold-way classification of topological insulators and topological superconductors according to three nonspatial symmetries: time-reversal, particle-hole, and chiral symmetry [4,5]. Soon after, it is found that, with additional spatial symmetries, topological invariants may have simplified expressions [6], or even the topological classification is enriched [7]. Recently, topological properties of dynamical [8–11] and open quantum-mechanical systems [12–15] are also studied extensively.

Since Haldane pointed out that topological band theory is not tied to fermions, but essentially wave effects [16], there are many works focusing on topological phenomena in other physical systems, such as magnonic crystals [17–19], photonic crystals [20–22], phononic crystal [23–25], and even coupled pendula [26]. Here we will focus on topology of collective modes in the weakly interacting ultracold bosonic atoms loaded in an optical lattice. It has been known that wave functions of the excited modes above Bose-Einstein condensates (BEC) can exhibit a topological structure [27–29]. However, all of these previous works focus on systems *breaking* time-reversal symmetry, which have a nonvanishing first Chern number in two dimensions that is in one-to-one correspondence with the number of chiral edge states dictated

by the bulk-boundary correspondence. This type of excitation band topology is analogous to the Chern insulators in class A.

It is well known that there is a topological phase protected by the odd time-reversal symmetry in two and three dimensions due to Kane and Mele [30], namely the topological insulators in class AII. This topological phase possesses a pair of helical edge states propagating in opposite directions, whose presence or absence is characterized by a \mathbb{Z}_2 index, which has many equivalent definitions, e.g., relating to the Pfaffian [30], the time reversal polarization [31], and the Wannier center flow [32]. The last one is of the most practical use, since it does not involve any gauge-fixing problems that occur in the previous two definitions. One natural question to ask is whether a similar topological structure exists in the excitation spectrum of a bosonic superfluid; if so, what type of symmetry protects them, how to define the associated bulk topological invariant, and whether the bulk-boundary correspondence still holds or not.

In this work, we show that a AII-class-like topological structure indeed exists in the Bogoliubov excitations of a BEC in an optical lattice, which is protected by a pseudo-time-reversal symmetry that is pseudo-antiunitary and squares to minus one. The corresponding bulk topological index is also a \mathbb{Z}_2 number, and three equivalent definitions used in the fermionic case all have counterparts here.

To address the problem in a systematical way that can be generalized easily for various kinds of symmetry-protected topological bosonic Bogoliubov bands, we review the problem of quadratic bosons in Sec. II, where we also introduce the Krein-space theory to reformulate the problem in a way that has the closest connection to its fermionic counterpart. In Sec. III, we show that a pseudo-time-reversal symmetry,

*jsw@mail.ustc.edu.cn

which is pseudo-antiunitary and squares to minus one, guarantees the bosonic Kramers' pair, which in turn protects a AII-class-like topological excitation spectrum. We then go on discussing three equivalent characterizations of the associated bulk \mathbb{Z}_2 topological invariant. Moreover, with an additional inversion symmetry, a simpler formula for it is derived. In Sec. IV, two toy models feasible in cold atom experiments are studied, and the bulk-boundary correspondence is confirmed numerically. In Sec. V we conclude the paper and give a discussion.

II. PRELIMINARY

A. Quadratic boson

Consider loading ultracold bosonic atoms in an optical lattice. In the weakly interacting region, atoms condense in the single-particle ground state. By employing the standard Bogoliubov–de Gennes approximation, the excitation of the condensate can be well described by a bosonic quadratic Hamiltonian, whose most general form in real space reads

$$H = \sum_{\mathbf{r}, \mathbf{r}'} \sum_{\alpha\beta} a_{\mathbf{r}\alpha}^\dagger A_{\mathbf{r}\alpha, \mathbf{r}'\beta} a_{\mathbf{r}'\beta} + \frac{1}{2} \sum_{\mathbf{r}, \mathbf{r}'} \sum_{\alpha\beta} (a_{\mathbf{r}\alpha}^\dagger B_{\mathbf{r}\alpha, \mathbf{r}'\beta} a_{\mathbf{r}'\beta}^\dagger + a_{\mathbf{r}\beta} B_{\mathbf{r}\alpha, \mathbf{r}'\beta}^* a_{\mathbf{r}'\alpha}), \quad (1)$$

where the bosonic creation (annihilation) operators $a_{\mathbf{r}\alpha}^\dagger$, labeled by an external index \mathbf{r} (assuming total M unit cells) and an internal index $\alpha \in 1, 2, \dots, N$, satisfy the canonical commutation relations (CCRs) $[a_{\mathbf{r}\alpha}, a_{\mathbf{r}'\beta}^\dagger] = \delta_{\mathbf{r}\mathbf{r}'} \delta_{\alpha\beta}$ and $[a_{\mathbf{r}\alpha}, a_{\mathbf{r}'\beta}] = [a_{\mathbf{r}\alpha}^\dagger, a_{\mathbf{r}'\beta}^\dagger] = 0$. Using a single index, one can write a and a^\dagger as MN -dimensional arrays and A and B as $MN \times MN$ matrices. We then have $A = A^\dagger$ due to Hermiticity of H and $B^T = B$ due to Bose statistics. Further introducing the Nambu spinor $\alpha = \begin{pmatrix} a \\ a^\dagger \end{pmatrix}$ and $\alpha^\dagger = (a^\dagger \ a)$, we can write Eq. (1) as

$$H = \frac{1}{2} \alpha^\dagger H_{\text{BdG}} \alpha, \quad H_{\text{BdG}} = \begin{pmatrix} A & B \\ B^* & A^T \end{pmatrix}, \quad (2)$$

where a constant term $\text{tr}A$ is omitted and the block matrix H_{BdG} is called the Bogoliubov–de Gennes (BdG) Hamiltonian. Because of the particle-hole constraint of Nambu spinor $\alpha = \Sigma_1 (\alpha^\dagger)^T$, where throughout this paper we denote $\Sigma_i = \sigma_i \otimes I_{MN}$, with σ_i ($i = 1, 2, 3$) being the standard Pauli matrices and I_{MN} being the $MN \times MN$ identity matrix (in momentum space it becomes I_N), the BdG Hamiltonian enjoys a particle-hole ‘‘symmetry’’ (PHS), $\mathcal{C}H_{\text{BdG}}\mathcal{C}^{-1} = H_{\text{BdG}}$, where $\mathcal{C} = \Sigma_1 K$ and K is the complex conjugation. In the presence of translation symmetry, i.e., $A_{\mathbf{r}\alpha, \mathbf{r}'\beta} = A_{\mathbf{r}-\mathbf{r}', \alpha\beta}$ and similarly for B , Eq. (2) can be written in momentum space as

$$H = \frac{1}{2} \sum_{\mathbf{k}} \alpha_{\mathbf{k}}^\dagger H_{\text{BdG}}(\mathbf{k}) \alpha_{\mathbf{k}}, \quad H_{\text{BdG}}(\mathbf{k}) = \begin{pmatrix} A_{\mathbf{k}} & B_{\mathbf{k}} \\ B_{-\mathbf{k}}^* & A_{-\mathbf{k}}^T \end{pmatrix}, \quad (3)$$

where the $2N$ -dimensional arrays are defined by

$$\alpha_{\mathbf{k}}^\dagger = (a_{\mathbf{k}1}^\dagger \dots a_{\mathbf{k}N}^\dagger \ a_{-\mathbf{k}1} \dots a_{-\mathbf{k}N}), \\ \alpha_{\mathbf{k}} = (a_{\mathbf{k}1} \dots a_{\mathbf{k}N} \ a_{-\mathbf{k}1}^\dagger \dots a_{-\mathbf{k}N}^\dagger)^T. \quad (4)$$

The $N \times N$ Hermitian matrix $A_{\mathbf{k}}$ has entries $[A_{\mathbf{k}}]_{\alpha\beta} = \sum_{\mathbf{r}} A_{\mathbf{r}-\mathbf{r}', \alpha\beta} e^{i\mathbf{k}\cdot\mathbf{r}}$ and similarly for the symmetric matrix $B_{\mathbf{k}}$. The PHS now reads $\mathcal{C}H_{\text{BdG}}(\mathbf{k})\mathcal{C}^{-1} = H_{\text{BdG}}(-\mathbf{k})$. In this representation, CCRs take a compact form

$$[\alpha_{\mathbf{k}a}, \alpha_{\mathbf{k}'b}^\dagger] = [\Sigma_3]_{ab} \delta_{\mathbf{k}, \mathbf{k}'}. \quad (5)$$

Equation (3) [and similarly for Eq. (2)] is solved by a Bogoliubov transformation

$$\beta_{\mathbf{k}} = T_{\mathbf{k}} \alpha_{\mathbf{k}}, \quad (6a)$$

$$\beta_{\mathbf{k}}^\dagger = \beta_{-\mathbf{k}}^T \Sigma_1 = \alpha_{\mathbf{k}}^\dagger \Sigma_1 T_{-\mathbf{k}}^T \Sigma_1, \quad (6b)$$

where the second equality in Eq. (6b) results from Eq. (6a). The transformation is assumed as follows. (i) To be canonical, i.e., the CCRs are preserved (double indices imply summation),

$$\begin{aligned} [\Sigma_3]_{ab} &= [\beta_{\mathbf{k}a}, \beta_{\mathbf{k}'b}^\dagger] \\ &= [T_{\mathbf{k}}]_{aa'} [\alpha_{\mathbf{k}a'}, \alpha_{\mathbf{k}'b'}^\dagger] [\Sigma_1 T_{-\mathbf{k}}^T \Sigma_1]_{b'b} \\ &= [T_{\mathbf{k}} \Sigma_3 \Sigma_1 T_{-\mathbf{k}}^T \Sigma_1]_{ab} \\ \Rightarrow i\Sigma_2 &= T_{\mathbf{k}} i \Sigma_2 T_{-\mathbf{k}}^T. \end{aligned} \quad (7)$$

Note the real space version of Eq. (7) is $i\Sigma_2 = Ti\Sigma_2T^T$, where Σ_2 and T are $MN \times MN$ matrices in this case. Hence the Bogoliubov transformations in real space form a complex symplectic group $\text{Sp}(2NM, \mathbb{C})$ [33]. (ii) To be unitary, i.e.,

$$\begin{aligned} (\beta_{\mathbf{k}a})^\dagger &= \beta_{\mathbf{k}a}^\dagger, \\ \alpha_{\mathbf{k}a'}^\dagger [T_{\mathbf{k}}^\dagger]_{a'a} &= \alpha_{\mathbf{k}a'}^\dagger [\Sigma_1 T_{-\mathbf{k}}^T \Sigma_1]_{a'a} \\ \Rightarrow T_{\mathbf{k}} &= \Sigma_1 T_{-\mathbf{k}}^* \Sigma_1. \end{aligned} \quad (8)$$

Combining Eq. (8) and Eq. (7), we further obtain

$$T_{\mathbf{k}} \Sigma_3 T_{\mathbf{k}}^\dagger \Sigma_3 = \Sigma_3 T_{\mathbf{k}}^\dagger \Sigma_3 T_{\mathbf{k}} = I_{2N}. \quad (9)$$

Matrices satisfying Eq. (9) are called paraunitary by Colpa [34]. (iii) The transformed Hamiltonian $H = \frac{1}{2} \beta_{\mathbf{k}}^\dagger \Sigma_3 T_{\mathbf{k}} \Sigma_3 H_{\text{BdG}}(\mathbf{k}) T_{\mathbf{k}}^{-1} \beta_{\mathbf{k}}$ is diagonal, i.e.,

$$\begin{aligned} T_{\mathbf{k}} \Sigma_3 H_{\text{BdG}}(\mathbf{k}) T_{\mathbf{k}}^{-1} \\ = \text{diag}[E_1(\mathbf{k}), \dots, E_N(\mathbf{k}), -E_1(-\mathbf{k}), \dots, -E_N(-\mathbf{k})], \end{aligned} \quad (10)$$

with $E_1(\mathbf{k}) \leq \dots \leq E_N(\mathbf{k})$. In this paper, we assume H_{BdG} is positive semidefinite, so that all eigenvalues are real [35]. Equation (10) indicates that one has to solve an eigenproblem of a generally *non-Hermitian* matrix [here only $H_{\text{BdG}}(\mathbf{k})$ itself is Hermitian by definition]

$$H_{\mathbf{k}}^{\text{eff}} = \Sigma_3 H_{\text{BdG}}(\mathbf{k}), \quad (11)$$

with a PHS,

$$\mathcal{C}H_{\mathbf{k}}^{\text{eff}}\mathcal{C}^{-1} = -H_{-\mathbf{k}}^{\text{eff}},$$

which guarantees that eigenvalues always come in pairs as shown in Eq. (10): for each eigenstate $|u_n^+(\mathbf{k})\rangle$ with nonnegative eigenvalue $E_n(\mathbf{k})$, called the particle excitation, we have another eigenstate, $|u_n^-(\mathbf{k})\rangle := \mathcal{C}|u_n^+(-\mathbf{k})\rangle = \Sigma_1 |u_n^+(-\mathbf{k})^*\rangle$, called the hole excitation, with nonpositive eigenvalue $-E_n(-\mathbf{k})$.

One may alternatively arrive at the effective Hamiltonian by examining the Heisenberg equations of motion for the operator $\alpha_{\mathbf{k}}(t)$ [36–38],

$$i \frac{d}{dt} \alpha_{\mathbf{k}a}(t) = [\alpha_{\mathbf{k}a}(t), H] = [\Sigma_3 H_{\text{BdG}}(\mathbf{k})]_{aa'} \alpha_{\mathbf{k}a'}(t),$$

where Eq. (5) is used in the second equality. Hence the dynamics of the system is indeed generated by the non-Hermitian matrix Eq. (11).

B. Krein space formalism

Here we review the basics of the Krein-space theory and reformulate the problem of quadratic boson using this language [39–41].

A Krein space (\mathcal{K}, J) is a Hilbert space \mathcal{K} with a *fundamental symmetry* J which is a linear operator satisfying $J^2 = 1$ and $J = J^\dagger$. Equivalently, operator J is a fundamental symmetry if

$$J^2 = 1, \quad \langle J\phi, J\psi \rangle = \langle \phi, \psi \rangle, \quad \forall \phi, \psi \in \mathcal{K},$$

where $\langle \cdot, \cdot \rangle$ is the usual inner product in the Hilbert space \mathcal{K} . A Krein space becomes real if there is a real structure and a real unitary Q which squares to ± 1 and (anti)commutes with J [42].

We define the *pseudo inner product* as

$$\langle\langle \phi, \psi \rangle\rangle := \langle \phi, J\psi \rangle. \quad (12)$$

It then follows that all familiar concepts defined with respect to the usual inner product have a pseudo-inner-product version. First of all, the *pseudo-adjoint* is defined by $A^\sharp = JA^\dagger J$, which by definition satisfies $\langle\langle A^\sharp \phi, \psi \rangle\rangle = \langle\langle \phi, A\psi \rangle\rangle$. Then the *pseudo-Hermitian* means $A^\sharp = A$, namely, Hermitian with respect to the pseudo inner product. *Pseudo-unitary* means $A^\sharp = A^{-1}$, namely, its pseudo-adjoint equals its inverse. *Pseudo-antiunitary* is antilinear with respect to the pseudo inner product, i.e., $\langle\langle A\phi, A\psi \rangle\rangle = \langle\langle \phi, \psi \rangle\rangle^* = \langle\langle \psi, \phi \rangle\rangle$. The *pseudo-orthogonal projector* is an operator that squares to itself and is pseudo-Hermitian, $\Pi^2 = \Pi = \Pi^\sharp$, which implies that Π and Π^\dagger are related by a similarity transformation.

Unlike Hermiticity, pseudo-Hermiticity does not guarantee reality of the spectrum. Nevertheless, the *Krein-spectral operator* H , defined by

$$\tilde{H} = UHU^{-1} = UHU^\sharp = \tilde{H}^\sharp = \tilde{H}^\dagger,$$

has real spectrum. Operators that are non-negative with respect to the pseudo inner product are automatically Krein spectral [34,39].

For the bosonic BdG system studied in this paper, we have the real Krein space of kind $(1, -1)$ [42] by setting $J = \Sigma_3$ and $Q = \Sigma_1$. The effective Hamiltonian Eq. (11) is pseudo-Hermitian with a real symmetry. The Bogoliubov transformation matrix $T_{\mathbf{k}}$ Eq. (6) is pseudo-unitary with a real symmetry.

Equation (9) can be rewritten using the pseudo inner product as

$$\begin{aligned} \langle\langle u_n^\pm(\mathbf{k}), u_m^\pm(\mathbf{k}) \rangle\rangle &= \pm \delta_{mn}, \\ \langle\langle u_n^\pm(\mathbf{k}), u_m^\mp(\mathbf{k}) \rangle\rangle &= 0, \end{aligned} \quad (13)$$

where $|u_n^\pm(\mathbf{k})\rangle$ is the right eigenstate of $H_{\mathbf{k}}^{\text{eff}}$ with eigenvalue $\pm E_n(\pm\mathbf{k})$. The pseudo-orthogonal projector, which is pseudo-

Hermitian and generally non-Hermitian, then takes the form

$$\Pi_{n,\mathbf{k}} = \pm |u_n^\pm(\mathbf{k})\rangle \langle u_n^\pm(\mathbf{k})| \Sigma_3. \quad (14)$$

From here on, unless otherwise stated, we will focus on the particle space since the hole excitations are just copies of the former due to PHS. To prevent cluttering, the superscript “+”, indicating states in particle space, will be omitted.

We briefly mention how to deal with the so-called Nambu-Goldstone (NG) modes in the context of topological band theory before proceeding further. The NG mode is a gapless mode due to spontaneously breaking a continuous symmetry. There are several types of NG modes; they may or may not satisfy the orthonormal conditions Eq. (13) [43,44]. Nevertheless, this type of mode can always be removed by adding an infinitesimal external field that explicitly breaks the corresponding symmetry. For example, the gapless phonon modes can open an infinitesimal gap by shifting the chemical potential in the negative direction, $\mu \rightarrow \mu - 0^+$. For simplicity, in this paper, we assume that the NG mode will have an infinitesimal gap. In fact, as will be discussed in the end of the next section, when considering the bulk-boundary correspondence to determine the helical midgap edge states, one may completely avoid discussing the topology relating to the lowest particle bands and highest hole bands (also see Ref. [27]).

III. \mathbb{Z}_2 INVARIANT ASSOCIATED WITH PSEUDO-TIME-REVERSAL SYMMETRY

A. Pseudo-time-reversal symmetry

For a bosonic system, the conventional time-reversal symmetry squares to $+1$ [45]. We define a pseudo-time-reversal (PTR) operator $\mathcal{T} = PK$ that squares to -1 . Here P is a \mathbf{k} -independent pseudo-unitary matrix. By definition, \mathcal{T} is pseudo-antiunitary [46].

A bosonic BdG system is said to respect the pseudo-time-reversal symmetry (PTRS) if

$$\mathcal{T} H_{\mathbf{k}}^{\text{eff}} \mathcal{T}^{-1} = H_{-\mathbf{k}}^{\text{eff}}. \quad (15)$$

Implications of PTRS for bosons resemble that of odd TRS for fermions: for every eigenstate $|u_n(\mathbf{k})\rangle$ of $H_{\mathbf{k}}^{\text{eff}}$, due to Eq. (15), $\mathcal{T}|u_n(-\mathbf{k})\rangle$ is also an eigenstate with eigenvalue $E(-\mathbf{k})$. At the pseudo-time-reversal-invariant momenta (PTRIM) Λ , these two states have the same eigenenergy and are orthogonal with respect to the pseudo inner product [19]. The orthogonality can be seen by considering $\langle\langle \mathcal{T}\phi, \mathcal{T}\psi \rangle\rangle = \langle\langle \psi, \phi \rangle\rangle$, which, upon setting $|\psi\rangle = |u_n(\Lambda)\rangle$ and $|\phi\rangle = \mathcal{T}|\psi\rangle$, has to vanish separately on both sides due to $\mathcal{T}^2 = -1$, leading to the orthogonality of the bosonic Kramers' pair, $|u_n(\Lambda)\rangle$ and $\mathcal{T}|u_n(\Lambda)\rangle$.

B. Pfaffian approach

Analogous to Kane and Mele's construction of the \mathbb{Z}_2 invariant [30], consider the matrix of overlaps with respect to the pseudo inner product $\langle\langle u_n(\mathbf{k}), \mathcal{T}u_m(\mathbf{k}) \rangle\rangle$, which is antisymmetric because \mathcal{T} is pseudo-antiunitary and squares to -1 . Assuming no other degeneracies, it is a 2×2 matrix and can be written as

$$\langle\langle u_n(\mathbf{k}), \mathcal{T}u_m(\mathbf{k}) \rangle\rangle = \epsilon_{nm} P(\mathbf{k}), \quad (16)$$

with $P(\mathbf{k})$ the Pfaffian of the matrix

$$P(\mathbf{k}) = \text{Pf}[\langle u_n(\mathbf{k}), \mathcal{T}u_m(\mathbf{k}) \rangle]. \quad (17)$$

Under a $U(2)$ transformation $|u_n(\mathbf{k})\rangle \rightarrow R_{nm}(\mathbf{k})|u_m(\mathbf{k})\rangle$, the Pfaffian becomes $P(\mathbf{k}) \rightarrow \det[R^*(\mathbf{k})]P(\mathbf{k})$ [cf. Eq. (A11)]. Thus $P(\mathbf{k})$ is invariant under a $SU(2)$ rotation but not $U(1)$, since the latter induces an overall phase factor. Nevertheless, $|P(\mathbf{k})|$ is $U(2)$ gauge invariant. At PTRIM Λ , due to the existence of a bosonic Kramers' pair, the off-diagonal element has unit modulus, namely $|P(\Lambda)| = 1$. We further define the unitary sewing matrix $B(\mathbf{k})$ that relates the PTR companion of an eigenstate at \mathbf{k} to another eigenstate at $-\mathbf{k}$,

$$|u_m(-\mathbf{k})\rangle = B_{mn}^*(\mathbf{k})\mathcal{T}|u_n(\mathbf{k})\rangle, \quad (18)$$

which leads to $P(-\mathbf{k}) = \det[B(\mathbf{k})]P^*(\mathbf{k})$ [cf. Eq. (A9)]. Thus whenever the Pfaffian vanishes at one momentum, so does the one at the opposite momentum with opposite ‘‘vorticity.’’ It then follows that the number of pairs of zeros of the Pfaffian is a \mathbb{Z}_2 invariant in the presence of PTRS, due to the same reason as in the fermionic case [30]. We hence conclude that the winding of the phase of $P(\mathbf{k})$ around a loop enclosing *half* the first Brillouin zone (1BZ),

$$I = \frac{1}{2\pi i} \oint_C d\mathbf{k} \cdot \nabla_{\mathbf{k}} \ln[P(\mathbf{k})],$$

is a \mathbb{Z}_2 invariant associated with PTRS for the bosonic BdG systems. It can be seen easily [cf. Eq. (A10)] that the Pfaffian in the particle bands and their hole companion has the same number of zeros, i.e., $I_{\text{particle}} = I_{\text{hole}}$.

C. Pseudo-time-reversal polarization

One can also define a pseudo-time-reversal polarization to characterize this \mathbb{Z}_2 invariant in analogous to Fu and Kane [31], which is also a straightforward generalization of the symplectic ‘‘charge’’ polarization constructed by Engelhardt and Brandes [47] for the bosonic BdG systems. Consider an effective one-dimensional (1D) system with k_2 (regarded as time t) fixed at $k_2 = 0$ or π ($t = 0$ or $T/2$), and set $k_1 = k$. Assuming no other degeneracies, N particle bands can be grouped into $N/2$ PTR pairs. The λ th ($\lambda = 1, 2, \dots, N/2$) pair for particle excitations are denoted by $|u_\lambda^{(l)}(\mathbf{k})\rangle$, with $l = 1, 2$ labeling the two states of the pair. Due to PTRS, for each pair, the PTR companion of an eigenstate with $l = 2$ at \mathbf{k} equals the eigenstate with $l = 1$ at $-\mathbf{k}$ up to a phase factor [31]

$$|u_\lambda^{(1)}(-k)\rangle = -e^{i\chi_{k,\lambda}}\mathcal{T}|u_\lambda^{(2)}(k)\rangle, \quad (19a)$$

$$|u_\lambda^{(2)}(-k)\rangle = e^{i\chi_{-k,\lambda}}\mathcal{T}|u_\lambda^{(1)}(k)\rangle, \quad (19b)$$

where the second equation results from the first one. We define the partial polarization for the λ th pair by

$$P_\lambda^{(l)} = \frac{1}{2\pi} \int_{-\pi}^{\pi} dk A_\lambda^{(l)}(k),$$

with the Berry connection [17]

$$A_\lambda^{(l)}(k) = i\langle u_\lambda^{(l)}(k), \partial_k u_\lambda^{(l)}(k) \rangle. \quad (20)$$

The sum of two partial polarizations is the symplectic generalization of ‘‘charge’’ polarization [47]. Here we consider their

difference,

$$\tilde{P}_\lambda = P_\lambda^{(1)} - P_\lambda^{(2)},$$

as the symplectic generalization of time-reversal polarization introduced by Fu and Kane [31], which satisfies (see Appendix B)

$$(-1)^{\tilde{P}_\lambda} = \frac{\sqrt{\det[B_\lambda(0)]} \sqrt{\det[B_\lambda(\pi)]}}{\text{Pf}[B_\lambda(0)] \text{Pf}[B_\lambda(\pi)]}, \quad (21)$$

where $B_\lambda(k) = B(k, 0)$ or $B(k, \pi)$ is the sewing matrix defined in Eq. (18) for the λ th pair, and the sign ambiguity of the square root is fixed by requiring that $\sqrt{B_\lambda(k)}$ is continuous for $k \in [0, \pi]$. Following the discussion in Ref. [31], the *change* in the PTR polarization during *half* the cycle, which physically tracks the difference between positions of the pairs of Wannier states, defines a \mathbb{Z}_2 invariant (i.e., whether the Wannier states ‘‘switch partners’’ or not),

$$\Delta_\lambda = \tilde{P}_\lambda(T/2) - \tilde{P}_\lambda(0) \pmod{2}. \quad (22)$$

Using Eq. (21), we may equivalently write Eq. (22) as

$$(-1)^{\Delta_\lambda} = \prod_{i=1}^4 \frac{\sqrt{\det[B_\lambda(\Gamma_i)]}}{\text{Pf}[B_\lambda(\Gamma_i)]}. \quad (23)$$

It is easily seen that Δ_λ is the same for particle bands and its hole companion, i.e., $\Delta_\lambda^{\text{particle}} = \Delta_\lambda^{\text{hole}}$ [cf. Eq. (A4)].

Incidentally, by enforcing the *pseudo-time-reversal constraint* [31],

$$|u_\lambda^{(1)}(-k, -t)\rangle = \mathcal{T}|u_\lambda^{(2)}(k, t)\rangle,$$

$$|u_\lambda^{(2)}(-k, -t)\rangle = -\mathcal{T}|u_\lambda^{(1)}(k, t)\rangle,$$

the \mathbb{Z}_2 invariant can also be interpreted as an obstruction. The resulting formula in terms of the Abelian Berry connection,

$$\mathbf{A}_\lambda(\mathbf{k}) = \sum_{l=1,2} i\langle u_\lambda^{(l)}(\mathbf{k}), \nabla_{\mathbf{k}} u_\lambda^{(l)}(\mathbf{k}) \rangle, \quad (24)$$

and the Abelian Berry curvature,

$$F_\lambda(\mathbf{k}) = \sum_{l=1,2} [\nabla_{\mathbf{k}} \times \mathbf{A}_\lambda^{(l)}(\mathbf{k})]_z,$$

has recently been proposed by Kondo *et al.* [19], which is defined by

$$\tilde{\Delta}_\lambda = \frac{1}{2\pi} \left\{ \oint_{\partial\text{HBZ}} d\mathbf{k} \cdot \mathbf{A}_\lambda(\mathbf{k}) - \int_{\text{HBZ}} d[2]k F_\lambda(\mathbf{k}) \right\} \pmod{2}, \quad (25)$$

where HBZ and ∂HBZ denote half the 1BZ and its boundary that does not have any two points related by PTRS. The proof that $\tilde{\Delta}_\lambda = \Delta_\lambda$ and their equivalence to the Pfaffian approach can be obtained similarly as given in the Appendix of Ref. [31].

D. \mathbb{Z}_2 invariant as Wannier center flow

All equivalent definitions of the \mathbb{Z}_2 invariant discussed so far suffer from the gauge-fixing problem. Here we generalize a practical Wilson loop approach proposed by Yu *et al.* [32]. It is extremely useful for numerics because it does not require any gauge-fixing condition.

Again consider the effective 1D system (with fixed k_2), we define the position operator $\hat{X} = \sum_{i\alpha} e^{i\delta_1 \cdot r_i} |i\alpha\rangle \langle i\alpha|$ as usual [48], where $|i\alpha\rangle = |i\rangle \otimes |\alpha\rangle = a_{r_i, \alpha}^\dagger |0\rangle$ and $\delta_1 = \mathbf{b}_1/N_1$, with \mathbf{b}_1 the primitive reciprocal vector and N_1 the number of unit cells for the effective 1D system. The Wannier states are given by the eigenstates of the position operator restricted in the occupied bands [49], $\hat{X}_P = \hat{P}\hat{X}\hat{P}$. Here the projection operator for the occupied subspace is [cf. Eq. (14)]

$$\hat{P} = \sum_{n \leq n_{\max}, k_1} |\psi_n(\mathbf{k})\rangle \langle \psi_n(\mathbf{k})| \Sigma_3,$$

where $|\psi_n(\mathbf{k})\rangle = |\mathbf{k}\rangle \otimes |u_n(\mathbf{k})\rangle$ is the Bloch eigenstate and $|\mathbf{k}\rangle = M^{-1/2} \sum_i e^{-i\mathbf{k} \cdot \mathbf{r}_i} |i\rangle$. Using

$$\langle\langle \psi_n(\mathbf{k}), \hat{X} \psi_{n'}(\mathbf{k}') \rangle\rangle = \delta_{\mathbf{k}+\delta_1, \mathbf{k}'} \langle\langle u_n(\mathbf{k}), u_{n'}(\mathbf{k} + \delta_1) \rangle\rangle,$$

the projected position operator can be written as

$$\begin{aligned} \hat{X}_P &= \sum_{n, n' \leq n_{\max}} \sum_{k_1} [\langle\langle u_n(\mathbf{k}), u_{n'}(\mathbf{k} + \delta_1) \rangle\rangle \\ &\quad \times |\psi_n(\mathbf{k})\rangle \langle \psi_{n'}(\mathbf{k} + \delta_1)| \Sigma_3]. \end{aligned}$$

We then raise \hat{X}_P to the N_1 th power,

$$\hat{X}_P^{N_1} = \sum_{m, n \leq n_{\max}} \sum_{k_1} [W_{\mathbf{k}}]_{mn} |\psi_m(\mathbf{k})\rangle \langle \psi_n(\mathbf{k})| \Sigma_3,$$

where the so-called *Wilson loop operator* $W_{\mathbf{k}}$ is defined by

$$W_{\mathbf{k}} = M^{(\mathbf{k}, \mathbf{k}+\delta_1)} M^{(\mathbf{k}+\delta_1, \mathbf{k}+2\delta_1)} \dots M^{[\mathbf{k}+(N_1-1)\delta_1, \mathbf{k}]}, \quad (26)$$

with $[M^{(\mathbf{k}, \mathbf{k}+\delta_1)}]_{mn} = \langle\langle u_m(\mathbf{k}), u_n(\mathbf{k} + \delta_1) \rangle\rangle$. In the limit $|\delta_1| \rightarrow 0$, we have $[M^{(\mathbf{k}, \mathbf{k}+\delta_1)}]_{mn} \rightarrow e^{-i[A_1(\mathbf{k})]_{mn} d k_1}$ with the non-Abelian $U(n_m)$ gauge field defined by

$$[A_1(\mathbf{k})]_{mn} = i \langle\langle u_m(\mathbf{k}), \partial_{k_1} u_n(\mathbf{k}) \rangle\rangle, \quad (27)$$

and Eq. (26) becomes the $U(n_m)$ Wilson loop, $W_{\mathbf{k}} = P \exp[\int_{-\pi}^{\pi} -i A_1(\mathbf{k}) d k_1]$ [50].

The eigenvalues of $W_{\mathbf{k}}$ are independent of k_1 and gauge invariant under a $U(n_m)$ gauge transformation of $|u_n(\mathbf{k})\rangle$ (see Appendix D). They are explicitly denoted by $w_n = |w_n| e^{i\theta_n}$, for $n = 1, \dots, n_{\max}$ with $\theta_n \in (-\pi, \pi]$. The eigenvalues of \hat{X}_P , as the N_1 th roots of w_n , read as $w_{n,j} = \exp[i\theta_n/N_1 + i2\pi j/N_1 + (\ln |w_n|)/N_1]$ for $j = 1, \dots, N_1$. Finally, the Wannier centers are identified with the phase of $w_{n,j}$,

$$\langle x \rangle_{n,j} = \frac{N_1}{2\pi} \arg w_{n,j} = \langle x \rangle_n + j, \quad \langle x \rangle_n = \theta_n/2\pi,$$

which is defined only up to a lattice translation.

Due to PTRS, eigenvalues of the Wilson loop operator at k_2 and $-k_2$ are the same; moreover, at PTRIM, eigenvalues are at least doubly degenerate (see Appendix D). Thus, starting from $k_2 = -\pi$, each Wannier center pair will split and recombine at $k_2 = 0$; and for $k_2 > 0$, the behavior is just the mirror of the former with respect to the $k_2 = 0$ plane. Due to the same reason as in the fermionic case [32], the sum of winding numbers for all $n_{\max}/2$ Wannier center pair is a \mathbb{Z}_2 invariant. The equivalence of this definition to all previous ones can be obtained, although tedious, similarly as given in the Appendix of Ref. [32].

E. Simplifications from inversion symmetry

Lastly, we show that, with an additional inversion symmetry (IS), the \mathbb{Z}_2 invariant Eq. (23) takes a simple form,

$$(-1)^{\Delta_\lambda} = \prod_i \xi_\lambda(\mathbf{A}_i), \quad (28)$$

where $\xi_\lambda(\mathbf{A}_i)$ is the parity eigenvalue of one of the λ th pair of bands at the PTRIM \mathbf{A}_i . Analogous to the fermionic case discussed by Fu and Kane [6], we explicitly construct a globally continuous transverse gauge where $\mathbf{A}_\lambda(\mathbf{k}) = 0$, and derive Eq. (28) in this gauge in the following.

A bosonic BdG system is said to respect IS, if there exists an inversion operator \mathcal{P} , such that

$$\mathcal{P} H_{\mathbf{k}}^{\text{eff}} \mathcal{P}^{-1} = H_{-\mathbf{k}}^{\text{eff}}.$$

Here, \mathcal{P} is assumed to be independent of \mathbf{k} , *pseudo-unitary*, *pseudo-Hermitian* [cf. Eqs. (A6) and (A7)], square to +1, and commute with \mathcal{T} . By definition, we have

$$\mathcal{P} \mathcal{T} H_{\mathbf{k}}^{\text{eff}} (\mathcal{P} \mathcal{T})^{-1} = H_{\mathbf{k}}^{\text{eff}},$$

i.e., all energy bands are at least doubly degenerate at each \mathbf{k} . It is also straightforward to show that, at PTRIM, each Kramers' pair has the same inversion eigenvalue; hence there is no ambiguity in choosing which one of the parity eigenvalues for the λ th pair in Eq. (28). Another immediate fact is that the Berry curvature $F_\lambda(\mathbf{k})$ must vanish since it is both odd and even in \mathbf{k} due to PTRS and IS, respectively. Now we define the unitary and antisymmetric sewing matrix C in an arbitrary gauge by

$$|u_m(\mathbf{k})\rangle = -C_{mn}^*(\mathbf{k}) \mathcal{P} \mathcal{T} |u_n(\mathbf{k})\rangle. \quad (29)$$

Assuming no other degeneracies, it is a 2×2 matrix labeled by λ . The Pfaffian of $C_\lambda(\mathbf{k})$ has unit magnitude and the gradient of its phase is related to the Berry connection Eq. (24) by (see Appendix C)

$$\mathbf{A}_\lambda(\mathbf{k}) = -\frac{i}{2} \text{tr}[C_\lambda^\dagger(\mathbf{k}) \nabla_{\mathbf{k}} C_\lambda(\mathbf{k})] = -i \nabla_{\mathbf{k}} \ln \text{Pf}[C_\lambda(\mathbf{k})]. \quad (30)$$

By setting $\text{Pf}[C_\lambda(\mathbf{k})] = 1$ via a suitable gauge transformation, the Berry connection vanishes. Due to [cf. Eq. (A8)]

$$C_\lambda(-\mathbf{k}) = B_\lambda(\mathbf{k}) C_\lambda^*(\mathbf{k}) B_\lambda^T(\mathbf{k}), \quad (31)$$

and $\text{Pf}[XAX^T] = \text{Pf}[A] \det[X]$, this gauge also guarantees that $\det[B_\lambda(\mathbf{k})] = 1$. Finally, from Eq. (A1), we have

$$[B(\mathbf{A}_i)]_{ll'} = \langle\langle \psi_\lambda^{(l)}(\mathbf{A}_i), \mathcal{P}(\mathcal{P}\mathcal{T})\psi_\lambda^{(l')}(\mathbf{A}_i) \rangle\rangle, \quad (32)$$

where $|\psi_\lambda^{(l)}(\mathbf{A}_i)\rangle = e^{i\mathbf{A}_i \cdot \mathbf{r}} |u_\lambda^{(l)}(\mathbf{A}_i)\rangle$ is the Bloch eigenstate. Since $[H, \mathcal{P}] = 0$, $|\psi_\lambda(\mathbf{A}_i)\rangle$ is also the eigenstate of \mathcal{P} with eigenvalue $\xi_\lambda = \pm 1$. Then using Eq. (A5), Eq. (32) leads to $B_\lambda(\mathbf{A}_i) = \xi_\lambda(\mathbf{A}_i) C_\lambda(\mathbf{A}_i)$, which gives $\text{Pf}[B_\lambda(\mathbf{A}_i)] = \xi_\lambda(\mathbf{A}_i) \text{Pf}[C_\lambda(\mathbf{A}_i)] = \xi_\lambda(\mathbf{A}_i)$ in the transverse gauge. All in all, we have $\sqrt{\det[B_\lambda(\mathbf{A}_i)]} / \text{Pf}[B_\lambda(\mathbf{A}_i)] = \xi_\lambda(\mathbf{A}_i)$, and Eq. (28) then follows from Eq. (23).

Finally, we note that, according to the bulk-boundary correspondence, the helical midgap edge states crossing at PTRIM is present (absent) if the \mathbb{Z}_2 index equals one (zero). For the case that the gap is between n th and $(n+1)$ th particle bands, the corresponding \mathbb{Z}_2 index is obtained by considering all bands below the $(n+1)$ th band, *including all hole bands*.

Since it has been shown that a pair of particle bands and its hole companion have the same \mathbb{Z}_2 index, one can equivalently sum all contributions *above* the n th particle bands. An additional merit of this treatment is that we hence avoid the ambiguity relating to the lowest particle bands (and highest hole bands), where the presence of Goldstone modes leads to undefined points in the Brillouin zone [27].

IV. TOY MODELS

We examine the topological properties of the excitation spectrum by calculating the bulk \mathbb{Z}_2 invariant in two ways (as an obstruction and as the Wannier center flow), and numerically verify the bulk-boundary correspondence for two toy models that are feasible in cold atom systems: the bosonic version of (1) the Kane-Mele model and (2) the Bernevig-Hughes-Zhang model. The former has PTRS but breaks IS in general, while the latter always preserves both. When IS exists, we also explicitly verify Eq. (28).

A. Bosonic Kane-Mele model

Our first example is a bosonic version of the Kane-Mele (BKM) model [30], which is a time-reversal-symmetric generalization of Haldane's honeycomb lattice model [51]. Since the latter has been realized in a cold atom experiment by Esslinger's group [52], we expect this model is ready for implementation. The noninteracting part of the Hamiltonian reads

$$H_0 = -t \sum_{\langle i,j \rangle} a_i^\dagger a_j - i\lambda_s \sum_{\langle\langle i,j \rangle\rangle} v_{ij} a_i^\dagger s_3 a_j - \lambda_v \sum_i \xi_i a_i^\dagger a_i, \quad (33)$$

where $a_i^{(\dagger)}$ is the bosonic annihilation (creation) operators at site i , with pseudospin index omitted. The first term describes the nearest-neighbor hopping; the second term describes the next-nearest-neighbor (NNN) complex hopping for both pseudospin sectors with an overall opposite sign between them (see Fig. 1). Here s_i (s_0), $i = 1, 2, 3$, is the standard Pauli (two-by-two identity) matrix acting on the pseudospin space. $v_{ij} = \text{sgn}(\mathbf{d}_i \times \mathbf{d}_j)_z = \pm 1$, with \mathbf{d}_i and \mathbf{d}_j along the two bonds constituting the next-nearest neighbors. The last term is a staggered sublattice potential $\xi_i = 1(-1)$ for $i \in A(B)$, which breaks IS of the system. The interacting part takes the form

$$H_{\text{int}} = \frac{U}{2} \sum_j \sum_{s=\uparrow,\downarrow} a_{js}^\dagger a_{js}^\dagger a_{js} a_{js}, \quad (34)$$

where the interspecies interactions are neglected for simplicity.

Using a primitive lattice vector as shown in Fig. 1, we write Eq. (33) in momentum space as $H_0 = \sum_{\mathbf{k}} a_{\mathbf{k}}^\dagger h(\mathbf{k}) a_{\mathbf{k}}$, where $a_i := (a_{iA\uparrow}, a_{iA\downarrow}, a_{iB\uparrow}, a_{iB\downarrow})^T$ and the 4-by-4 Bloch Hamiltonian reads

$$h(\mathbf{k}) = d_1(\mathbf{k})\Gamma_1 + d_2\Gamma_2 + d_{12}(\mathbf{k})\Gamma_{12} + d_{15}(\mathbf{k})\Gamma_{15}, \quad (35)$$

with the Clifford algebra generators

$$\Gamma_a = (\sigma_1 \otimes s_0, \sigma_3 \otimes s_0, \sigma_2 \otimes s_1, \sigma_2 \otimes s_2, \sigma_2 \otimes s_3), \quad (36)$$

and $\Gamma_{ab} = \frac{1}{2i}[\Gamma_a, \Gamma_b]$, where σ_i (s_0), $i = 1, 2, 3$, are the Pauli (two-by-two identity) matrix acting on the sublattice space.

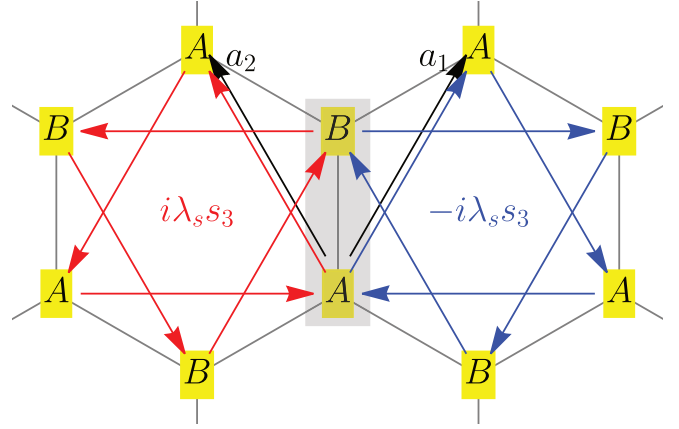


FIG. 1. Kane-Mele model on a honeycomb lattice. Two sublattices, highlighted in yellow, are denoted as A and B , with a unit cell indicated by the gray rectangle. \mathbf{a}_1 and \mathbf{a}_2 are the Bravais lattice vectors. The gray line denotes the NN hopping amplitude $-t$, while the NNN hopping matrix of Haldane's type are shown in red and blue with the arrow implying the hopping direction. Note the relative minus sign between two species of bosons are captured by the standard Pauli matrix s_3 acting on the pseudospin space.

All real parameters are listed in Table I. In this representation we have $\tilde{T}\Gamma_a\tilde{T}^{-1} = \Gamma_a$ and $\tilde{T}\Gamma_{ab}\tilde{T}^{-1} = -\Gamma_{ab}$, with

$$\tilde{T} = i(\sigma_0 \otimes s_2)K = -i\Gamma_{35}K. \quad (37)$$

Hence d_a (d_{ab}) is even (odd) in \mathbf{k} dictated by the odd TRS: $\tilde{T}h(\mathbf{k})\tilde{T}^{-1} = h(-\mathbf{k})$.

The single-particle band minimum obtained from Eq. (35) is the same as the Haldane model studied by Refs. [27,54]: for $|\lambda_s| < t/\sqrt{3}$, the band bottom locates at Γ , while for larger $|\lambda_s|$, the minimum jumps to the corners \mathbf{K}_A and \mathbf{K}_B of the first Brillouin zone (1BZ). Here we focus on the former case where the condensation is expected to occur at Γ . Then, by taking a general ground-state wave function ansatz and minimizing the corresponding Gross-Pitaevskii (GP) energy functional (see Appendix E), the superfluid order parameter is found to be $\langle a_{iA\uparrow} \rangle = \langle a_{iA\downarrow} \rangle = \cos(\bar{\theta}/2)\sqrt{n}/2$ and $\langle a_{iB\uparrow} \rangle = \langle a_{iB\downarrow} \rangle = \sin(\bar{\theta}/2)\sqrt{n}/2$, with $\bar{\theta}$ as a function of λ_v/t and Un/t (cf. Fig. 7).

Applying the standard Bogoliubov theory (see Appendix E), we obtain the effective Hamiltonian [note it is non-Hermitian due to the presence of imaginary i in the first line on the right-hand side (RHS)],

$$H_{\mathbf{k}}^{\text{eff}} = \tau_0 \otimes [d_{15}(\mathbf{k})\Gamma_{15}] + i\tau_2 \otimes (\tilde{d}_0\Gamma_0 + \tilde{d}_2\Gamma_2) + \tau_3 \otimes [d_0\Gamma_0 + d_1(\mathbf{k})\Gamma_1 + \tilde{d}_2\Gamma_2 + d_{12}(\mathbf{k})\Gamma_{12}], \quad (38)$$

TABLE I. Parameters used in Eq. (35) are given in the first two rows and extra parameters used in Eq. (38) are given in the last two rows, with $x = \sqrt{3}k_x a/2$ and $y = 3k_y a/2$. Note $\bar{\theta}$ itself is a function of λ_v/t and Un/t ; see Fig. 7.

d_1	$-t(1 + 2 \cos x \cos y)$	d_2	$-\lambda_v$
d_{12}	$2t \cos x \sin y$	d_{15}	$4\lambda_s(\cos x - \cos y) \sin x$
d_0	$\lambda_v \cos \bar{\theta} + 3t \sin \bar{\theta} + \frac{1}{4}nU \sin^2 \bar{\theta}$	\tilde{d}_0	$\frac{1}{4}nU$
\tilde{d}_2	$-\lambda_v + \frac{1}{2}nU \cos \bar{\theta}$	\tilde{d}_2	$\frac{1}{4}nU \cos \bar{\theta}$

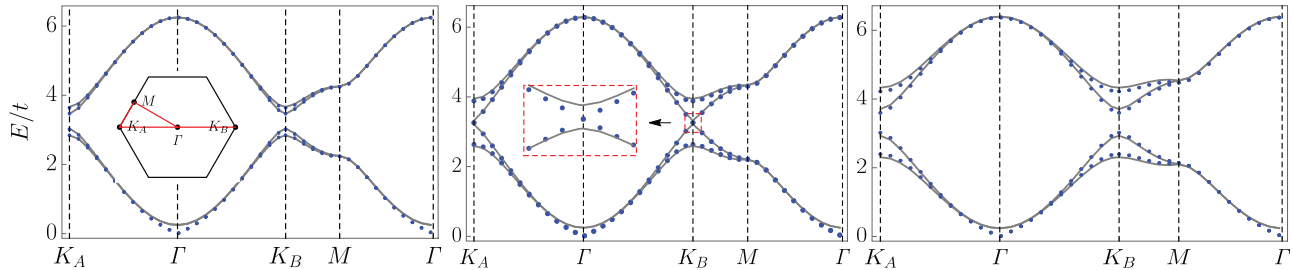


FIG. 2. Bogoliubov excitation spectrum (blue dots) under full periodic boundary conditions along high symmetric lines in the 1BZ (shown in the inset of the left figure) for (left) $\lambda_v/t = 0.10$, (middle) $\lambda_v/t = \lambda_v^*/t \approx 0.36$, and (right) $\lambda_v/t = 0.70$. The noninteracting bands (shifted upwards by $nU/2 - \mu$) are also plotted in gray solid lines. As shown in the inset of the middle figure, when the gap of Bogoliubov excitation spectrum just closes, the corresponding gap of the noninteracting band has already reopened again. Other relevant parameters: $nU/t = 1$ and $\lambda_s/t = 0.06$.

where $\Gamma_0 = \sigma_0 \otimes s_0$ and all real parameters are listed in Table I. One can easily see that this effective Hamiltonian has PTRS with the PTR operator

$$\mathcal{T} = \tau_0 \otimes \tilde{\mathcal{T}}.$$

Diagonalization of Eq. (38) leads to the Bogoliubov excitation spectrum shown in Fig. 2 along the high symmetric lines. In the low energy limit, there are two Goldstone modes resulting from the spontaneous breaking of two $U(1)$ symmetries corresponding to particle number and s_3 conservations, respectively.

For the noninteracting Hamiltonian, Eq. (35), the system is gapped for a general λ_v at half filling. The gap-closing-and-reopening transition occurs at two corners \mathbf{K}_A and \mathbf{K}_B when $\lambda_v = \pm 3\sqrt{3}\lambda_s$ [30]. This behavior is smoothly carried over to the Bogoliubov excitation spectrum, with the only difference that now $\lambda_v = \lambda_v^* \neq \pm 3\sqrt{3}\lambda_s$. By calculating eigenvalues of $H_{\mathbf{K}_A}^{\text{eff}}$ (or equivalently $H_{\mathbf{K}_B}^{\text{eff}}$) and equating the second and third eigenvalues, the critical value λ_v^* is found to be a function of λ_v/t and nU/t , which is plotted as blue dots in Fig. 3(a). For the case with $\lambda_s, nU \ll t$, it takes the form

$$\lambda_v^* \approx 3\sqrt{3}\lambda_s + \frac{\sqrt{3}}{2}\lambda_s nU/t, \quad (39)$$

which indeed returns to the noninteracting case by setting $U = 0$. Using Eq. (25) with the numerical method of Fukui and Hatsugai [53], for the higher pair of particle bands, we find $\tilde{\Delta}_2 = 1$ for $|\lambda_v| < \lambda_v^*$, corresponding to the \mathbb{Z}_2 topological region, and $\tilde{\Delta}_2 = 0$ for $|\lambda_v| > \lambda_v^*$, corresponding to the \mathbb{Z}_2 trivial region. We also calculate the Wannier center flow for the higher pair of particle bands [Figs. 3(d) and 3(e)], and the Bogoliubov excitations in a one-dimensional zigzag strip [Figs. 3(b) and 3(c)], which confirms the equivalence of two definitions of the \mathbb{Z}_2 invariant, and the bulk-boundary correspondence (i.e., the presence or absence of helical edge states for the \mathbb{Z}_2 topological or trivial region).

For $\lambda_v = 0$, we have $\tilde{\theta} = \pi/2$, and the effective Hamiltonian enjoys IS with the inversion operator $\mathcal{P} = \tau_0 \otimes \Gamma_1$. At four PTRIM, we find

$$(\xi_{00}, \xi_{01}, \xi_{10}, \xi_{11}) = (-1, -1, -1, 1),$$

where ξ_{ij} is the eigenvalue of \mathcal{P} for the second pair of particle bands at PTRIM $\mathbf{k} = i\mathbf{b}_1/2 + j\mathbf{b}_2/2$. Equation (28) then indi-

cates that the case with $\lambda_v = 0$ is in the \mathbb{Z}_2 topological region, as expected.

As seen both from Eq. (39) (in a specific limit) and from Fig. 3(a), the \mathbb{Z}_2 topological region becomes larger with increasing the interaction strength (or the particle number density). To understand why this is the case physically, we first note that the large λ_v limit corresponds to the ‘‘atomic limit’’ [55], where all atoms are tightly located at one of the two sublattices, corresponding to an extreme sublattice imbalance, and is of course \mathbb{Z}_2 trivial. By turning on a large $|\lambda_v|$ from zero (i.e., from the \mathbb{Z}_2 topological region), one encounters a gap-closing-and-reopening transition. Effects of the repulsive interaction, on the other hand, suppress the sublattice imbalance induced by λ_v , since it favors a uniform configuration. As a result, to reach the critical value of sublattice imbalance, one needs a larger λ_v .

B. Bosonic Bernevig-Hughes-Zhang model

Our second example is a bosonic version of the Bernevig-Hughes-Zhang (BBHZ) model, which is a time-reversal-symmetric generalization of the Chern insulator on the square lattice. Motivated by a scheme proposed by Liu *et al.* [56], which has been experimentally realized by Pan’s group [57,58], we consider two copies (labeled by $\eta = A, B$) of pseudospin-1/2 (labeled by $s = \uparrow, \downarrow$) bosons on the square lattice, with the tight-binding Hamiltonian (Fig. 4)

$$H_0 = -t \sum_{(i,j)} a_i^\dagger (\eta_0 \otimes s_0) a_j - m_z \sum_i a_i^\dagger (\eta_0 \otimes s_3) a_i - t_s \sum_{(i,j)} a_i^\dagger h_s^{ij} a_j, \quad (40)$$

where $a_{i\eta s}^{(\dagger)}$ is the annihilation (creation) operator of η boson with pseudospin s at site \mathbf{r}_i and $a_i := (a_{iA\uparrow}, a_{iA\downarrow}, a_{iB\uparrow}, a_{iB\downarrow})^T$. η_i (η_0) and s_i (s_0), $i = 1, 2, 3$, are Pauli (two-by-two identity) matrices acting on boson-copy space and pseudospin space, respectively. t denotes pseudospin-conserved hopping; m_z is a constant Zeeman term. The pseudospin-flip hopping matrix h_s^{ij} is shown explicitly in Fig. 4. Note the relative minus sign, i.e., the presence of η_3 , between two copies of bosons when they hop along the x direction, makes Eq. (40) odd time-reversal symmetric [59]. The interacting part of the

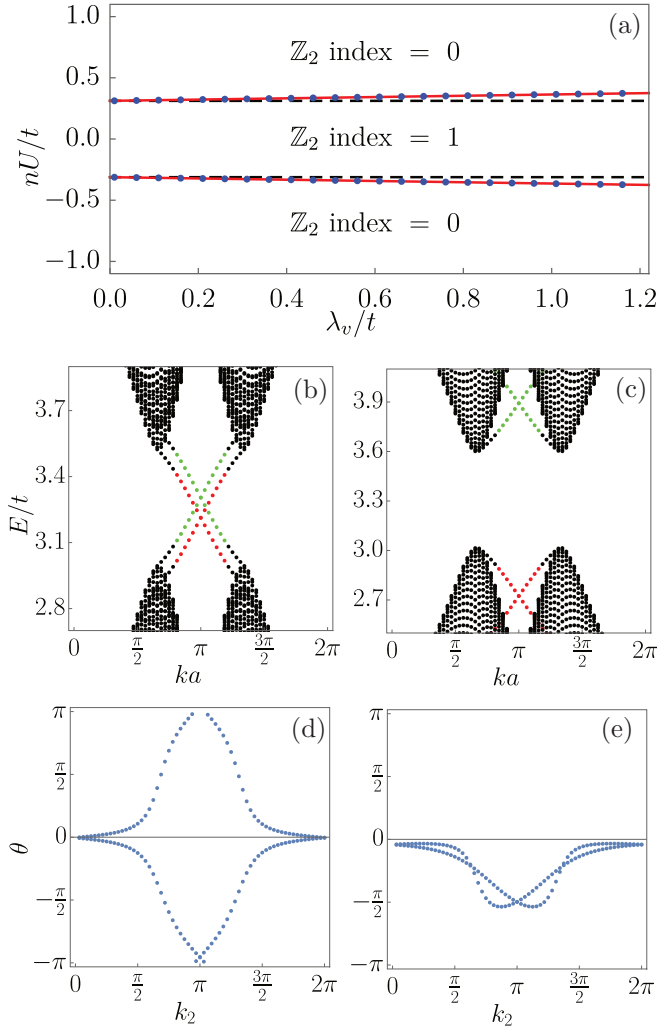


FIG. 3. (a) \mathbb{Z}_2 index, calculated using Eq. (25) and the numerical method of [53], for the higher two particle bands in the BKM model with $nU/t = 1$ and $\lambda_v/t = 0.06$. The boundaries, shown in blue dotted lines, are obtained via a full numerical calculation [explained above Eq. (39)]. Red solid lines are obtained from the series expansion, Eq. (39). Comparing with the black dashed vertical lines (corresponding to the noninteracting case) shows that the \mathbb{Z}_2 topological region becomes larger. In (b) $\lambda_v/t = 0.1$ and (c) $\lambda_v/t = 0.7$, we zoom in around the midgap of the Bogoliubov excitation spectrum of particle bands in a strip geometry of 64 unit cells (each with 64 sites) with zigzag edges. Red (green) points correspond to edge modes, whose wave functions have more than 80% weight on the leftmost (rightmost) unit cell. Panels (d) and (e) are the corresponding Wannier center flow of the second pair of particle bands by treating k_2 as the time.

Hamiltonian takes the same form as Eq. (34) for each copy of boson.

After a gauge transformation $a_{j\eta\downarrow} \rightarrow (-1)^j a_{j\eta\downarrow}$ [56], the momentum-space Bloch Hamiltonian is

$$h(\mathbf{k}) = \eta_0 \otimes \{[-2t(\cos k_x + \cos k_y) - m_z]s_3 - 2t_s \sin k_x s_2\} + \eta_3 \otimes (-2t_s \sin k_y s_1), \quad (41)$$

which resembles the four-band model for HgTe introduced by Bernevig, Hughes, and Zhang [60]. This single-particle

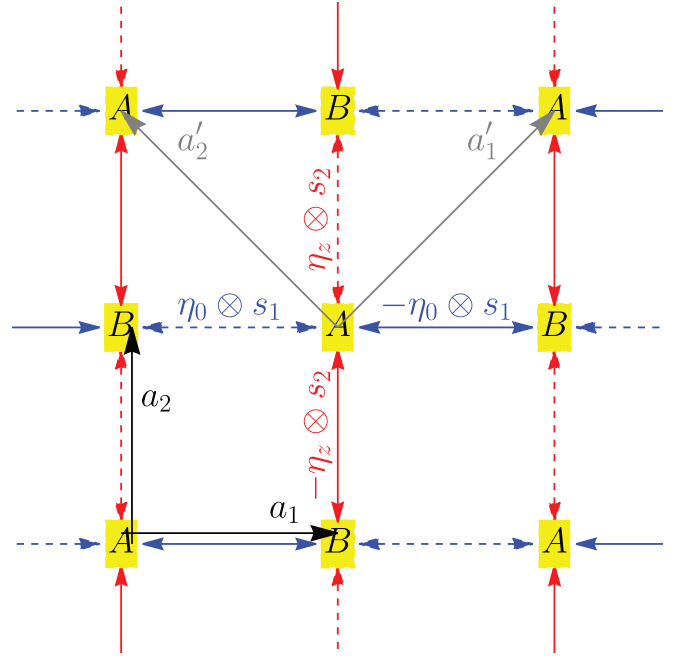


FIG. 4. Bernevig-Hughes-Zhang-like model on a square lattice. It is a straightforward generalization of the scheme proposed by Liu *et al.* [56]. The pseudospin-flip hopping matrix h_s^{ij} along x (y) direction, used in Eq. (40), are shown in blue (red), with the arrow indicating the hopping direction. There is a relative minus sign between dashed lines and solid lines of the same color. Hence, in the original gauge, the unit cell contains two sites (denoted as A and B with yellow background), with the corresponding Bravais primitive lattice vector $\mathbf{a}'_{1,2}$ shown in gray [61]. Only *after* performing a clever gauge transformation $a_{j\eta\downarrow} \rightarrow (-1)^j a_{j\eta\downarrow}$ [56], all lines become solid, and it is then valid to use $\mathbf{a}_{1,2}$ shown in black, as the two Bravais lattice vectors, and the unit cell contains only a single site.

Hamiltonian has both odd TRS

$$\tilde{\mathcal{T}}h(\mathbf{k})\tilde{\mathcal{T}}^{-1} = h(-\mathbf{k}), \quad \tilde{\mathcal{T}} = i\eta_2 \otimes s_0 K,$$

and IS

$$\tilde{\mathcal{P}}h(\mathbf{k})\tilde{\mathcal{P}}^{-1} = h(-\mathbf{k}), \quad \tilde{\mathcal{P}} = \eta_0 \otimes s_3.$$

Instead of Eq. (36), it is convenient to choose the Dirac matrices to be even under $\tilde{\mathcal{P}}\tilde{\mathcal{T}}$ [6],

$$\Gamma_a = (\eta_0 \otimes s_3, \eta_0 \otimes s_2, \eta_1 \otimes s_1, \eta_2 \otimes s_1, \eta_3 \otimes s_1).$$

Then $\tilde{\mathcal{T}} = -i\Gamma_{35}K$, $\tilde{\mathcal{P}} = \Gamma_1$, and the commutators are odd under $\tilde{\mathcal{P}}\tilde{\mathcal{T}}$, i.e., $\tilde{\mathcal{P}}\tilde{\mathcal{T}}\Gamma_{ab}(\tilde{\mathcal{P}}\tilde{\mathcal{T}})^{-1} = -\Gamma_{ab}$. Due to $\Gamma_1 = \tilde{\mathcal{P}}$, we further have

$$\tilde{\mathcal{T}}\Gamma_a\tilde{\mathcal{T}} = \tilde{\mathcal{P}}\Gamma_a\tilde{\mathcal{P}} = \begin{cases} +\Gamma_a & \text{for } a = 1, \\ -\Gamma_a & \text{for } a \neq 1. \end{cases}$$

Equation (41) is then recast into

$$h(\mathbf{k}) = d_1(\mathbf{k})\Gamma_1 + d_2(\mathbf{k})\Gamma_2 + d_5(\mathbf{k})\Gamma_5, \quad (42)$$

with all real coefficients listed in Table II. As shown in Ref. [6], the \mathbb{Z}_2 invariant for this noninteracting model can be identified using the same formula as Eq. (28). The representation of Dirac matrices has been chosen such that, at the four TRIM, only d_1 can be nonzero, i.e., $h(\mathbf{\Lambda}) = d_1(\mathbf{\Lambda})\tilde{\mathcal{P}}$. Hence one can directly obtain all eigenvalues of $\tilde{\mathcal{P}}$ for the occupied

TABLE II. Parameters used in Eq. (42) are given in the first two rows and extra parameters used in Eq. (44) are given in the last two rows.

d_1	$-2t(\cos k_x + \cos k_y) - m_z$	d_2	$-2t_s \sin k_x$
d_5	$-2t_s \sin k_y$		
\tilde{d}_1	$\frac{nU}{2} + d_1$	d_0	$\frac{nU}{4}$
\tilde{d}_0	$4t + m_z$		

bands,

$$(\xi_{00}, \xi_{01}, \xi_{10}, \xi_{11}) = (-4t - m_z, -m_z, -m_z, 4t - m_z), \quad (43)$$

which shows that the noninteracting system is in the \mathbb{Z}_2 topological region for $|m_z| < 4t$, and in the \mathbb{Z}_2 trivial region otherwise.

Single-particle bands of Eq. (41) are the same as the Chern insulator with a twofold degeneracy dictated by $\tilde{\mathcal{P}}\tilde{\mathcal{T}}$ symmetry. For $|t_s| < t_s^*$, where $t_s^* = \sqrt{2t^2 + m_z t}/2$, the band minimum locates at Γ (\mathbf{M}) if $m_z > 0$ ($m_z < 0$). For $|t_s| > t_s^*$, this single minimum splits into four points, $(\pm k_0, \pm k_0)$ with $k_0 = \arccos \frac{m_z t}{2(t_s^2 - 2t^2)}$. Here we will focus on the former case, and assume bosons condense *only* at Γ , by taking a sufficiently large positive m_z . Then, using a general ground-state wavefunction ansatz and minimizing the corresponding GP energy functional (see Appendix E), the superfluid order parameter is found to be $\langle a_{iA\uparrow} \rangle = \langle a_{iB\uparrow} \rangle = 1/\sqrt{2}$ and $\langle a_{iA\downarrow} \rangle = \langle a_{iB\downarrow} \rangle = 0$, for the physically relevant region (cf. Fig. 9).

Using the Bogoliubov theory, we obtain the effective Hamiltonian (note it is non-Hermitian due to the presence of imaginary i in the first line on the RHS) (see Appendix E),

$$H_{\mathbf{k}}^{\text{eff}} = d_5 \tau_0 \otimes \Gamma_5 + id_0 \tau_2 \otimes (\Gamma_0 + \Gamma_1) \\ \times \tau_3 \otimes (\tilde{d}_0 \Gamma_0 + \tilde{d}_1 \Gamma_1 + d_2 \Gamma_2), \quad (44)$$

with $\Gamma_0 = \eta_0 \otimes s_0$ and all real parameters listed in Table II. It is straightforward to check that this effective Hamiltonian has both PTRS with the PTR operator

$$\mathcal{T} = \tau_0 \otimes \tilde{\mathcal{T}} \quad (45)$$

and IS with the inversion operator

$$\mathcal{P} = \tau_0 \otimes \tilde{\mathcal{P}}. \quad (46)$$

Diagonalization of Eq. (44) leads to the Bogoliubov excitation spectrum shown in Fig. 5, which is doubly degenerate

dictated by \mathcal{PT} symmetry. In the low energy limit, there are two Goldstone modes due to the spontaneous breaking of two U(1) symmetries associated to particle number and η_3 conservations, respectively.

For the noninteracting Hamiltonian Eq. (42), the gap-closing-and-reopening transition occurs at \mathbf{M} when $m_z = 4t$ for m_z positive [cf. Eq. (43)]. This behavior is again smoothly carried over to the Bogoliubov excitation spectrum, with the only difference that now $m_z = m_z^* \neq 4t$. By calculating eigenvalues of $H_{\mathbf{M}}^{\text{eff}}$ and equating the two relevant ones, we find

$$m_z^* = \sqrt{2t(8t + nU)} + \frac{nU}{4}, \quad (47)$$

which indeed returns to the noninteracting case by setting $U = 0$. Using Eq. (25) with the numerical method of Fukui and Hatsugai [53], for the higher pair of particle bands, we find $\tilde{\Delta}_2 = 1$ for $m_z < m_z^*$, corresponding to the \mathbb{Z}_2 topological region, while $\tilde{\Delta}_2 = 0$ for $m_z > m_z^*$, corresponding to the \mathbb{Z}_2 trivial region. We also calculate the Wannier center flow for the higher pair of particle bands, and the Bogoliubov excitations in a strip geometry as shown in Fig. 6, which confirms the equivalence of two definitions of the \mathbb{Z}_2 invariant and the bulk-boundary correspondence.

Since this model always has IS, we may simply examine the parity eigenvalues at the PTRIM. Because the gap closes only at \mathbf{M} , the parity eigenvalues can only change there. We thus consider the eigenvalues of two relevant particle bands with the corresponding eigenstates at \mathbf{M} (note $E_{l+1} = E_l$ for $l = 1, 2$):

$$E_1(\mathbf{M}) = \sqrt{8t(8t + nU)}, \quad E_3(\mathbf{M}) = 2m_z - \frac{nU}{2}, \\ |u_1(\mathbf{M})\rangle \propto \left(0, 0, -\frac{16t + nU + 4\sqrt{2t(8t + nU)}}{nU}, \right. \\ \left. 0, 0, 0, 1, 0 \right)^T, \\ |u_3(\mathbf{M})\rangle = (0, 0, 0, 1, 0, 0, 0)^T.$$

which are obviously also the eigenvectors of inversion operator with parity 1 and -1 , respectively. Hence the topological transition occurs at the degeneracy point $E_1(\mathbf{M}) = E_3(\mathbf{M})$ which leads again to Eq. (47). To determine the presence or absence of helical edge modes between the first and second pair of particle bands, one has to find out all four eigenvalues

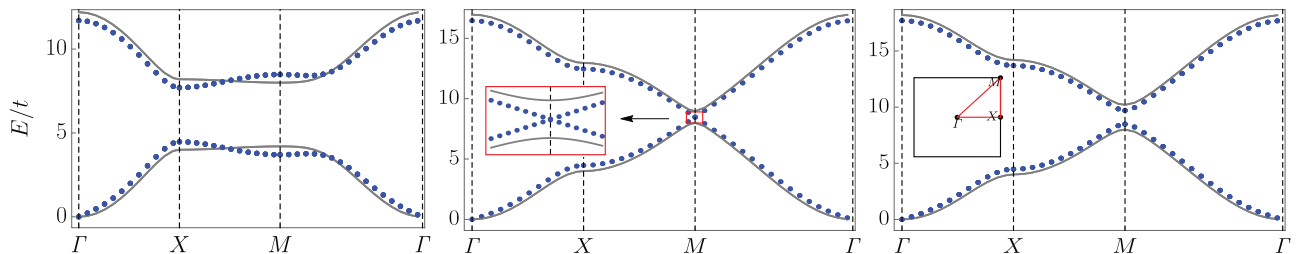


FIG. 5. Bogoliubov excitation spectrum (blue dots) under full periodic boundary conditions along high symmetric lines in the 1BZ (shown in the inset of the right figure), for (left) $m_z/t = 2.10$, (middle) $m_z/t = m_z^*/t \approx 4.48$, and (right) $m_z/t = 5.10$. The noninteracting bands (shifted upwards by $nU/2 - \mu$) are also plotted in gray lines. As shown in the inset of the middle figure, when the gap of Bogoliubov excitation spectrum just closes, the gap corresponding to the noninteracting band has already reopened. Other relevant parameters: $nU/t = t_s/t = 1$.

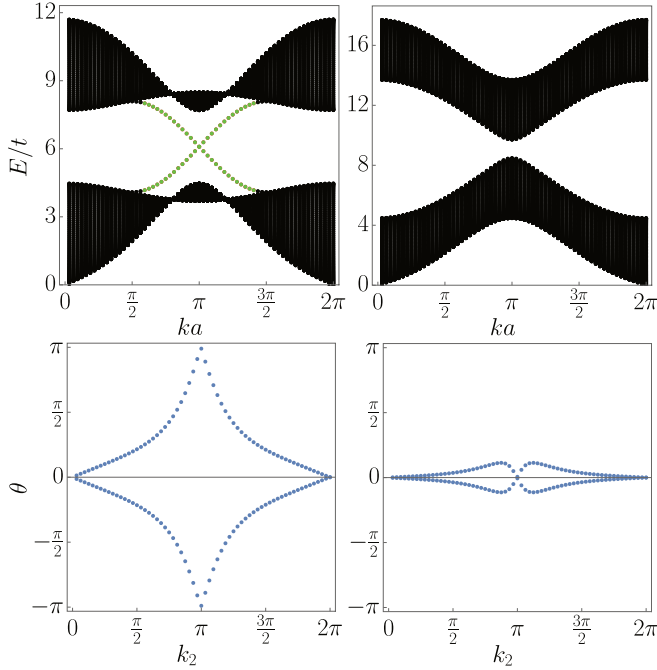


FIG. 6. Bogoliubov excitation spectrum of particle bands in a strip geometry of 64 unit cells (each containing 64 sites) for $m_z/t = 2.1$ (left top) and $m_z/t = 5.1$ (right top). Green points correspond to edge modes, whose wave functions have more than 80% weight on the rightmost unit cell. Edge modes on the leftmost unit cell completely overlap with the green points due to IS. The corresponding Wannier center flow of the second pair of particle bands by treating k_2 as the time is shown in the bottom. Other relevant parameters: $nU/t = t_s/t = 1$.

of \mathcal{P} for the second pair of bands at PTRIM,

$$(\xi_{00}, \xi_{01}, \xi_{10}, \xi_{11}) = (-1, 1, 1, 1), \quad \text{for } m_z < m_z^*.$$

Equation (28) then indicates that $m_z < m_z^*$ corresponds to the \mathbb{Z}_2 topological region, while $m_z > m_z^*$ is the \mathbb{Z}_2 trivial region, as expected.

Lastly, we note that the \mathbb{Z}_2 topological region of the BBHZ model also becomes larger with increasing the interaction strength (or the particle number density), as seen from Eq. (47). Similar to the BKM model, physically speaking, the repulsive interaction favors a uniform configuration, which suppresses the pseudospin imbalance induced by m_z . In turn, to reach the critical value of pseudospin imbalance, one needs a larger m_z , i.e., the \mathbb{Z}_2 topological region becomes larger.

V. CONCLUSION AND DISCUSSION

In this article, we studied topological Bogoliubov excitations in BEC in optical lattices protected by a PTRS that is analogous to topological insulators in class AII of fermions. The bulk topological \mathbb{Z}_2 invariant is shown to be characterized by the Pfaffian, the pseudo-time-reversal polarization, and the Wannier center flow. The last definition is most useful because it is gauge independent. With an additional inversion symmetry, this \mathbb{Z}_2 invariant can be identified by examining the inversion eigenvalues of the “occupied” states at PTRIM. In two simple and experimentally feasible examples, we con-

firmed the bulk-boundary correspondence numerically, and found in both cases that the topological region is enlarged by the interaction or the particle number density, since the repulsive interaction favors a uniform configuration which suppresses the effects of sublattice (pseudospin) imbalance induced by λ_v (m_z), which will lead a transition to the topological trivial region. Effectively, this topology becomes more “robust.”

Similar to the fermionic case discussed in Ref. [62], we expect that the topological properties discussed in this paper should be robust against weak disorder that (1) respect the PTRS and (2) are sufficiently weak so that topological excitation band gap does not close and the system does not enter into the Bose glass phase (where the topology of excitation spectrum could change dramatically). Of course, a more serious study should be carried out in the future.

The bulk-boundary correspondence guarantees that a non-trivial \mathbb{Z}_2 index implies the existence of topological edge states which can be experimentally detected in cold atom experiments [63–66]. We expect the topological helical edge modes discussed here can be probed in a similar manner. To experimentally measure the topological properties of the Bogoliubov excitations, one can also coherently transfer a small portion of the condensate into an edge mode using Raman transitions [67], and a density wave should be formed along the edge due to an interference with the background condensate [27].

One straightforward generalization of our work is to consider a AII-class-like excitation band topology of BEC in three dimensions [68,69]. Using the language of Krein-space theory developed in this paper, one may also consider various (symmorphic or nonsymmorphic) crystalline-symmetry-protected excitation band topology of weakly interacting BEC in optical lattices in the superfluid phase, analogous to its fermionic counterpart [70]. One may also study excitations in the Mott insulator phase, where similar topological structure is expected to occur [54,71].

Lastly, we note that, despite the well-known effectiveness of the Bogoliubov theory to the weakly interacting bosons, it is interesting to go beyond this approximation and consider higher-order quantum corrections, by using either exact numerical methods or many-body perturbation theory. The fate of PTRS and the associated topological properties could be studied further in the future.

ACKNOWLEDGMENTS

Y.D. acknowledges the support by National Natural Science Foundation of China (under Grant No. 11625522) and the National Key R&D Program of China (under Grants No. 2016YFA0301604 and No. 2018YFA0306501).

APPENDIX A: PROPERTIES OF TWO SEWING MATRICES AND PFAFFIAN

For the sewing matrix B defined in Eq. (18), one can find its explicit matrix elements as follows:

$$\begin{aligned} \langle\langle u_m(-\mathbf{k}), \mathcal{T}u_n(\mathbf{k}) \rangle\rangle &= -\langle\langle u_n(\mathbf{k}), \mathcal{T}u_m(-\mathbf{k}) \rangle\rangle \\ &= \langle\langle u_n(\mathbf{k}), B_{ml}(\mathbf{k})u_l(\mathbf{k}) \rangle\rangle \\ &= B_{mn}(\mathbf{k}). \end{aligned} \quad (\text{A1})$$

It then follows that B is *unitary* (double indices imply summation),

$$\begin{aligned} B_{mn}(\mathbf{k})B_{ln}^*(\mathbf{k}) &= \langle\langle u_m(-\mathbf{k}), \mathcal{T}u_n(\mathbf{k}) \rangle\rangle \langle\langle u_l(-\mathbf{k}), \mathcal{T}u_n(\mathbf{k}) \rangle\rangle^* \\ &= \langle\langle u_n(\mathbf{k}), \mathcal{T}u_m(-\mathbf{k}) \rangle\rangle \langle\langle \mathcal{T}u_l(-\mathbf{k}), u_n(\mathbf{k}) \rangle\rangle \\ &= \langle \mathcal{T}u_l(-\mathbf{k}) | \Sigma_3 | u_n(\mathbf{k}) \rangle \langle u_n(\mathbf{k}) | \Sigma_3 | \mathcal{T}u_m(-\mathbf{k}) \rangle \\ &= \langle\langle \mathcal{T}u_l(-\mathbf{k}), \mathcal{T}u_m(-\mathbf{k}) \rangle\rangle \\ &= \langle\langle u_m(-\mathbf{k}), u_l(-\mathbf{k}) \rangle\rangle \\ &= \delta_{ml}, \end{aligned} \quad (\text{A2})$$

and has the property $B_{mn}(\mathbf{k}) = -B_{nm}(-\mathbf{k})$ since

$$\begin{aligned} B_{mn}(\mathbf{k}) &= \langle\langle u_m(-\mathbf{k}), \mathcal{T}u_n(\mathbf{k}) \rangle\rangle \\ &= -\langle\langle u_n(\mathbf{k}), \mathcal{T}u_m(-\mathbf{k}) \rangle\rangle \\ &= -B_{nm}(-\mathbf{k}). \end{aligned} \quad (\text{A3})$$

The sewing matrix for hole bands is related to its particle companion by

$$\begin{aligned} [B_{\text{hole}}]_{mn}(\mathbf{k}) &= \langle\langle \Sigma_1 u_m^*(\mathbf{k}), \mathcal{T} \Sigma_1 u_n(-\mathbf{k})^* \rangle\rangle \\ &= \pm \langle\langle u_m(\mathbf{k}), \mathcal{T}u_n(-\mathbf{k}) \rangle\rangle^* \\ &= \pm B_{mn}^*(-\mathbf{k}), \end{aligned} \quad (\text{A4})$$

where \pm corresponds to $P = \tau_3 \otimes M$ or $\tau_0 \otimes M$ with τ_i (τ_0), $i = 1, 2, 3$, the standard Pauli (two-by-two identity) matrix, and the Hermitian matrix M satisfying $MM^* = -1$. In particular, for the two examples studied in Sec. IV, the minus sign is picked.

For the sewing matrix C defined in Eq. (29), one can find its explicit matrix elements as follows:

$$\begin{aligned} \langle\langle u_m(\mathbf{k}), \mathcal{P} \mathcal{T} u_n(\mathbf{k}) \rangle\rangle &= -\langle u_m(\mathbf{k}) | \Sigma_3 C_{nl} (\mathcal{P} \mathcal{T})^2 u_l(\mathbf{k}) \rangle \\ &= C_{nl} \langle\langle u_m(\mathbf{k}), u_l(\mathbf{k}) \rangle\rangle \\ &= C_{mn}. \end{aligned} \quad (\text{A5})$$

It then follows that C is *unitary*,

$$\begin{aligned} C_{mn}(\mathbf{k})C_{ln}^*(\mathbf{k}) &= \langle\langle u_m(\mathbf{k}), \mathcal{P} \mathcal{T} u_n(\mathbf{k}) \rangle\rangle \langle\langle u_l(\mathbf{k}), \mathcal{P} \mathcal{T} u_n(\mathbf{k}) \rangle\rangle^* \\ &= \langle\langle \mathcal{P} u_n(\mathbf{k}), \mathcal{T} u_m(\mathbf{k}) \rangle\rangle \langle\langle \mathcal{T} u_l(\mathbf{k}), \mathcal{P} u_n(\mathbf{k}) \rangle\rangle \\ &= \langle \mathcal{T} u_l(\mathbf{k}) | \Sigma_3 \mathcal{P} | u_n(\mathbf{k}) \rangle \langle u_n(\mathbf{k}) | \mathcal{P} \Sigma_3 \mathcal{T} | u_m(\mathbf{k}) \rangle \\ &= \langle \mathcal{T} u_l(\mathbf{k}) | \Sigma_3 \mathcal{T} | u_m(\mathbf{k}) \rangle \\ &= \langle\langle u_m(\mathbf{k}), u_l(\mathbf{k}) \rangle\rangle \\ &= \delta_{ml}, \end{aligned} \quad (\text{A6})$$

where we used *pseudo-unitarity* of \mathcal{P} , and C is *antisymmetric*,

$$\begin{aligned} C_{mn}(\mathbf{k}) &= \langle\langle u_m(\mathbf{k}), \mathcal{P} \mathcal{T} u_n(\mathbf{k}) \rangle\rangle \\ &= -\langle\langle \mathcal{P} u_n(\mathbf{k}), \mathcal{T} u_m(\mathbf{k}) \rangle\rangle \\ &= -\langle\langle u_n(\mathbf{k}), \mathcal{P} \mathcal{T} u_m(\mathbf{k}) \rangle\rangle \\ &= -C_{nm}, \end{aligned} \quad (\text{A7})$$

where we used *pseudo-Hermiticity* of \mathcal{P} . One can relate C at \mathbf{k} and $-\mathbf{k}$ using B :

$$\begin{aligned} C_{mn}(-\mathbf{k}) &= \langle\langle u_m(-\mathbf{k}), \mathcal{P} \mathcal{T} u_n(-\mathbf{k}) \rangle\rangle \\ &= B_{ml}(\mathbf{k}) \langle\langle \mathcal{T} u_l(\mathbf{k}), \mathcal{P} \mathcal{T}^2 u_l(\mathbf{k}) \rangle\rangle B_{nl'}(\mathbf{k}) \\ &= B_{ml}(\mathbf{k}) \langle\langle u_l(\mathbf{k}), \mathcal{P} \mathcal{T} u_{l'}(\mathbf{k}) \rangle\rangle^* B_{nl'}(\mathbf{k}) \\ &= B_{ml}(\mathbf{k}) C_{l'l}^*(\mathbf{k}) [B^T(\mathbf{k})]_{l'n}, \end{aligned} \quad (\text{A8})$$

which leads to Eq. (31). Similarly, one can relate the Pfaffian P at \mathbf{k} and $-\mathbf{k}$ using B :

$$\begin{aligned} P(-\mathbf{k}) &= \text{Pf}[\langle\langle u_n(-\mathbf{k}), \mathcal{T} u_m(-\mathbf{k}) \rangle\rangle] \\ &= \text{Pf}[B_{nl}(\mathbf{k}) \langle\langle \mathcal{T} u_{l'}(\mathbf{k}), u_l(\mathbf{k}) \rangle\rangle B_{ml'}(\mathbf{k})] \\ &= \text{Pf}[B_{nl}^*(\mathbf{k}) \langle\langle u_l(\mathbf{k}), \mathcal{T} u_{l'}(\mathbf{k}) \rangle\rangle B_{ml'}^*(\mathbf{k})]^* \\ &= \det[B(\mathbf{k})] P^*(\mathbf{k}). \end{aligned} \quad (\text{A9})$$

The Pfaffian for the hole bands is also related to its particle companion,

$$\begin{aligned} P_{\text{hole}}(\mathbf{k}) &= \text{Pf}[\langle\langle \Sigma_1 u^*(-\mathbf{k}), \mathcal{T} \Sigma_1 u_m^*(-\mathbf{k}) \rangle\rangle] \\ &= \pm \text{Pf}[\langle\langle u^*(-\mathbf{k}), \mathcal{T} u_m^*(-\mathbf{k}) \rangle\rangle] \\ &= \pm \text{Pf}[\langle\langle u(-\mathbf{k}), \mathcal{T} u_m(-\mathbf{k}) \rangle\rangle]^* \\ &= \pm P(-\mathbf{k})^* \\ &= \pm \det[B(\mathbf{k})]^* P(\mathbf{k}), \end{aligned} \quad (\text{A10})$$

where again \pm corresponds to $P = \tau_3 \otimes M$ or $\tau_0 \otimes M$.

Lastly, considering a gauge transformation only in particle space $|u_n(\mathbf{k})\rangle \rightarrow R_{nm}(\mathbf{k})|u_m(\mathbf{k})\rangle$, to preserve the orthonormal condition with respect to the pseudo inner product, R has to be unitary. It then follows that the Pfaffian becomes

$$\begin{aligned} P(\mathbf{k}) &\rightarrow \text{Pf}[R_{nl}^*(\mathbf{k}) \langle\langle u_l(\mathbf{k}), \mathcal{T} u_{l'}(\mathbf{k}) \rangle\rangle R_{ml'}(\mathbf{k})] \\ &= \det[R^*(\mathbf{k})] P(\mathbf{k}). \end{aligned} \quad (\text{A11})$$

The sewing matrix B becomes

$$B_{mn}(\mathbf{k}) \rightarrow [R^*(-\mathbf{k})]_{ml} B_{ll'}(\mathbf{k}) [R^\dagger(\mathbf{k})]_{l'n} \quad (\text{A12})$$

and the sewing matrix C becomes

$$C_{mn}(\mathbf{k}) \rightarrow [R^*(\mathbf{k})]_{ml} C_{ll'}(\mathbf{k}) [R^\dagger(\mathbf{k})]_{l'n}. \quad (\text{A13})$$

APPENDIX B: PROOF OF EQ. (21)

We first relate the Berry connection between two states of the λ th pair using Eq. (19),

$$\begin{aligned} A_\lambda^{(1)}(-k) &= -i \langle\langle \partial_k \mathcal{T} u_\lambda^{(1)}(-k), \mathcal{T} u_\lambda^{(1)}(-k) \rangle\rangle \\ &= -i \langle\langle \partial_k u_\lambda^{(2)}(k), u_\lambda^{(2)}(k) \rangle\rangle + \partial_k \chi_{k,\lambda} \\ &= A_\lambda^{(2)}(k) + \partial_k \chi_{k,\lambda}. \end{aligned} \quad (\text{B1})$$

Then the partial polarization for $l = 1$ can be written as

$$\begin{aligned} P_\lambda^{(1)} &= \frac{1}{2\pi} \int_0^\pi dk [A_\lambda^{(1)}(k) + A_\lambda^{(1)}(-k)] \\ &= \frac{1}{2\pi} \left[\int_0^\pi dk A_\lambda(k) + (\chi_{\pi,\lambda} - \chi_{0,\lambda}) \right], \end{aligned} \quad (\text{B2})$$

where $A_\lambda(k) = A_\lambda^{(1)}(k) + A_\lambda^{(2)}(k)$ is the full (Abelian) Berry connection. Using the sewing matrix B and the representation Eq. (19), we have $\frac{\text{Pf}[B_\lambda(\pi)]}{\text{Pf}[B_\lambda(0)]} = e^{-i\chi_{\pi,\lambda} + i\chi_{0,\lambda}}$; hence Eq. (B2) becomes

$$P_\lambda^{(1)} = \frac{1}{2\pi} \left[\int_0^\pi dk A_\lambda(k) + i \ln \left(\frac{\text{Pf}[B(\pi)]}{\text{Pf}[B(0)]} \right) \right]. \quad (\text{B3})$$

Under a $U(1)$ gauge transformation $|u_\lambda^{(l)}(k)\rangle \rightarrow e^{i\tilde{\chi}(k)} |u_\lambda^{(l)}(k)\rangle$, both terms on the RHS of Eq. (B3) induce $2\tilde{\chi}(\pi) - 2\tilde{\chi}(0)$ with *opposite* sign, thus canceling each other. By writing the

full Berry connection as the trace of the U(2) non-Abelian Berry connection [cf. Eq. (27)], $A_\lambda(k) = \text{Tr} \mathcal{A}_\lambda(k)$, the first term on the RHS of Eq. (B3) is manifestly invariant under a SU(2) gauge transformation $|u_\lambda^{(l)}(k)\rangle \rightarrow U_{l'l''}(k)|u_\lambda^{(l'')}(k)\rangle$; for the second term, due to Eq. (A12), the Pfaffian at the PTRIM transforms as $\text{Pf}[B(k)] \rightarrow \text{Pf}[B(k)] \det[U^*]$ and is also invariant. We conclude that $P_\lambda^{(1)}$ is U(2) invariant analogous to

the fermionic case [31]. Similarly, one can find that $P_\lambda^{(2)} = \frac{1}{2\pi} [\int_{-\pi}^0 dk A_\lambda(k) - i \ln \left(\frac{\text{Pf}[B(\pi)]}{\text{Pf}[B(0)]} \right)]$; hence the symplectic generalization of charge polarization reads

$$P_\lambda = P_\lambda^{(1)} + P_\lambda^{(2)} = \frac{1}{2\pi} \int_{-\pi}^\pi dk A_\lambda(k). \quad (\text{B4})$$

Using the sewing matrix B , we massage Eq. (B4) at $k_2 = -\pi$,

$$\begin{aligned} P_\lambda(k_2 = -\pi) &= \frac{i}{2\pi} \int_{-\pi}^\pi dk \sum_{l=1}^2 \langle\langle u_\lambda^{(l)}(k, -\pi), \partial_k u_\lambda^{(l)}(k, -\pi) \rangle\rangle \\ &= -\frac{i}{2\pi} \int_{-\pi}^\pi dk \sum_{l=1}^2 \langle\langle u_\lambda^{(l)}(-k, -\pi), \partial_k u_\lambda^{(l)}(-k, -\pi) \rangle\rangle \\ &= \frac{1}{2\pi} \int_{-\pi}^\pi dk \text{Tr} [B_\lambda^*(k, \pi) \mathcal{A}_\lambda(k, \pi) B_\lambda^T(k, \pi)] + \frac{i}{2\pi} \int_{-\pi}^\pi dk \text{Tr} [B_\lambda^\dagger(k, \pi) \partial_k B_\lambda(k, \pi)] \\ &= P_\lambda(k_2 = \pi) + \frac{i}{2\pi} \int_{-\pi}^\pi dk \partial_k \ln \det B_\lambda(k, \pi) \\ &= P_\lambda(k_2 = \pi). \end{aligned} \quad (\text{B5})$$

Hence the *change* of charge polarization under a cycle of k_2 from $-\pi$ to π vanishes, which is nothing but the fact that the Chern number vanishes for a 2D PTR symmetric system. We then consider the symplectic generalization of PTR polarization,

$$\tilde{P}_\lambda = P_\lambda^{(1)} - P_\lambda^{(2)} = \frac{1}{2\pi} \left\{ \int_0^\pi dk A_\lambda(k) - \int_{-\pi}^0 dk A_\lambda(k) + 2i \ln \left(\frac{\text{Pf}[B(\pi)]}{\text{Pf}[B(0)]} \right) \right\}. \quad (\text{B6})$$

We massage the middle term on the RHS of Eq. (B6) using the sewing matrix B ,

$$\begin{aligned} \int_{-\pi}^0 dk A_\lambda(k) &= -\frac{i\xi_\lambda}{2\pi} \int_0^\pi dk \sum_{l=1}^2 \langle\langle u_\lambda^{(l)}(-k), \partial_k u_\lambda^{(l)}(-k) \rangle\rangle \\ &= \frac{1}{2\pi} \int_0^\pi dk \text{Tr} [B_\lambda^*(k) \mathcal{A}_\lambda(k) B_\lambda^T(k)] + \frac{i}{2\pi} \int_0^\pi \text{Tr} [B^\dagger(k) \partial_k B(k)] \\ &= \frac{1}{2\pi} \int_0^\pi dk A_\lambda(k) - \frac{1}{2\pi i} \int_0^\pi dk \partial_k \ln \det B(k). \end{aligned} \quad (\text{B7})$$

Hence Eq. (B6) becomes

$$\tilde{P}_\lambda = \frac{1}{\pi i} \left[\int_0^\pi dk \partial_k \ln \sqrt{\det[B(k)]} - \ln \left(\frac{\text{Pf}[B(\pi)]}{\text{Pf}[B(0)]} \right) \right], \quad (\text{B8})$$

which leads to Eq. (21).

APPENDIX C: PROOF OF EQ. (30)

We directly massage the definition of Berry connection using the sewing matrix C ,

$$\begin{aligned} A_\lambda(\mathbf{k}) &= i \sum_{l=1,2} \langle\langle u_\lambda^{(l)}(\mathbf{k}), \nabla_{\mathbf{k}} u_\lambda^{(l)}(\mathbf{k}) \rangle\rangle \\ &= i \sum_{l=1,2} C_{l'l''}(\mathbf{k}) \langle\langle \mathcal{P} T u_{l'}(\mathbf{k}), \nabla_{\mathbf{k}} \mathcal{P} T u_{l''}(\mathbf{k}) \rangle\rangle C_{l''l}^*(\mathbf{k}) \\ &\quad + i \sum_{l=1,2} C_{l'l''}(\mathbf{k}) \langle\langle \mathcal{P} T u_{l'}(\mathbf{k}), \mathcal{P} T u_{l''}(\mathbf{k}) \rangle\rangle \nabla_{\mathbf{k}} C_{l''l}^*(\mathbf{k}) \end{aligned}$$

$$\begin{aligned} &= -\text{tr} C^* \mathcal{A}_\lambda^*(\mathbf{k}) C^T - i \text{tr} C^\dagger(\mathbf{k}) \nabla_{\mathbf{k}} C(\mathbf{k}) \\ &= -A_\lambda(\mathbf{k}) - i \text{tr} C^\dagger(\mathbf{k}) \nabla_{\mathbf{k}} C(\mathbf{k}), \end{aligned}$$

which leads to the first line of Eq. (30). The second line then follows from the identity $\nabla \ln \det[U] = \text{tr}[\nabla \ln U] = \text{tr}[U^\dagger \nabla U]$, valid for any unitary matrix U .

APPENDIX D: PROPERTIES OF WILSON LOOP OPERATOR

Suppose $|w\rangle$ is an eigenvector of the Wilson loop operator $W_{\mathbf{k}}$ with the eigenvalue w , i.e., $W_{\mathbf{k}}|w\rangle = w|w\rangle$. For any \mathbf{k}' ,

which satisfies $\mathbf{k}' = n\delta_1 + \mathbf{k}$ (without loss of generality $0 \leq n \leq N_1$), we have

$$\begin{aligned} & w M^{[\mathbf{k}' - N_1 \delta_1, \mathbf{k}' - (N_1 - 1) \delta_1]} M^{[\mathbf{k}' - (N_1 - 1) \delta_1, \mathbf{k}' - (N_1 - 2) \delta_1]} \\ & \dots M^{[\mathbf{k}' - (n+1) \delta_1, \mathbf{k}' - n \delta_1]} |w\rangle \\ & = M^{[\mathbf{k}' - N_1 \delta_1, \mathbf{k}' - (N_1 - 1) \delta_1]} M^{[\mathbf{k}' - (N_1 - 1) \delta_1, \mathbf{k}' - (N_1 - 2) \delta_1]} \\ & \dots M^{[\mathbf{k}' - (n+1) \delta_1, \mathbf{k}' - n \delta_1]} W_{\mathbf{k}} |w\rangle \\ & = W_{\mathbf{k}'} M^{(\mathbf{k}', \mathbf{k}' + \delta_1)} M^{(\mathbf{k}' + \delta_1, \mathbf{k}' + 2\delta_1)} \dots M^{(\mathbf{k} - \delta_1, \mathbf{k})} |w\rangle. \end{aligned}$$

Hence $W_{\mathbf{k}'}$ also has the same eigenvalue w . Namely, *eigenvalues of $W_{\mathbf{k}}$ are independent of k_1* .

One may write the Wilson loop operator in terms of a non-Hermitian projector,

$$W_{\mathbf{k}} = \Pi_0 \Pi_1 \dots \Pi_{N_1},$$

where $\Pi_l = \sum_{n \leq n_{\max}} |u_n(\mathbf{k} + l\delta_1)\rangle \langle u_n(\mathbf{k} + l\delta_1)| \Sigma_3$ is the projector to the occupied subspace and the entries of $W_{\mathbf{k}}$ are given by $[W_{\mathbf{k}}]_{mn} = \langle u_m(\mathbf{k}), W_{\mathbf{k}} u_n(\mathbf{k}) \rangle$. It is therefore manifestly $U(n_m)$ gauge invariant.

Since eigenvalues of $W_{\mathbf{k}}$ are independent of k_1 , without loss of generality, we may consider a particular Wilson loop operator

$$W_{k_2} = \Pi_{-k_1/2, k_2} \Pi_{-k_1/2 + \delta_1, k_2} \dots \Pi_{k_1/2, k_2},$$

where $\Pi_{k_1, k_2} = \sum_{n \leq n_{\max}} |u_n(k_1, k_2)\rangle \langle u_n(k_1, k_2)| \Sigma_3$. Using the sewing matrix B , we have

$$\begin{aligned} \Pi_{-k_1, -k_2} & = \sum_{n \leq n_{\max}} |u_n(-k_1, -k_2)\rangle \langle u_n(-k_1, -k_2)| \Sigma_3 \\ & = \sum_{n, l, l' \leq n_{\max}} B_{nl}^* (\mathbf{k}) P |u_l^*(k_1, k_2)\rangle \langle u_{l'}^*(k_1, k_2)| P^\dagger \Sigma_3 B_{nl'} \\ & = P \Pi_{k_1, k_2}^* P^{-1} \\ & = P \Sigma_3 \Pi_{k_1, k_2}^T \Sigma_3 P^{-1}, \end{aligned} \quad (\text{D1})$$

where we used the unitarity of B and the pseudo-unitarity of P . It follows that the Wilson loop at $-k_2$ and at k_2 are related,

$$\begin{aligned} W_{-k_2} & = \Pi_{-k_1/2, -k_2} \Pi_{-k_1/2 + \delta_1, -k_2} \dots \Pi_{k_1/2, -k_2} \\ & = P \Sigma_3 \Pi_{k_1/2, k_2}^T \Pi_{k_1/2 - \delta_1, k_2}^T \dots \Pi_{k_1/2, k_2}^T \Sigma_3 P^{-1} \\ & = P \Sigma_3 W_{k_2}^T \Sigma_3 P^{-1}. \end{aligned} \quad (\text{D2})$$

Since eigenvalues remain the same under both the transpose and the similarity transformations, *the Wilson loop at k_y and $-k_y$ have the same eigenvalues*.

At $k_2 = 0$ or π , the 1D effective Hamiltonian is PTR symmetric; therefore, each eigenstate $|\psi\rangle$ has a PTR companion $\mathcal{T}|\psi\rangle$ with the same energy and that are orthogonal with respect to the pseudo inner product,

$$\langle\langle \psi, \mathcal{T}\psi \rangle\rangle = \langle \psi | \Sigma_3 P K \psi \rangle = 0. \quad (\text{D3})$$

These states are also the eigenstates of the Wilson loop $W = W_0$ or W_π . Using Eq. (D2) and pseudo-unitarity of P , we have

$$\begin{aligned} w |\psi\rangle & = W |\psi\rangle \\ & = P \Sigma_3 P^\dagger \Sigma_3 W P \Sigma_3 P^\dagger \Sigma_3 |\psi\rangle \\ & = P \Sigma_3 W^T P^\dagger \Sigma_3 |\psi\rangle. \end{aligned}$$

Multiplying both sides from the left by P^* , then taking the complex conjugation, we have

$$\begin{aligned} w^* P K |\psi\rangle & = \Sigma_3 W^\dagger (P^{-1})^\dagger \Sigma_3 K |\psi\rangle \\ \Leftrightarrow w^* \Sigma_3 P K |\psi\rangle & = W^\dagger \Sigma_3 P K |\psi\rangle, \end{aligned} \quad (\text{D4})$$

where we used $PP^* = -1$ and again pseudo-unitarity of P . Since Eq. (D4) shows that the Wilson loop W has a left eigenvector with eigenvalue w^* which is orthogonal to $|\psi\rangle$ due to Eq. (D3), *the right eigenvalue w must be at least twice degenerate at $k_2 = 0$ or π* .

Lastly, we note that the Wilson loop operator for the hole bands is related to its particle companion, $W_{\mathbf{k}}^{\text{hole}} = \Sigma_1 (W_{-\mathbf{k}}^{\text{particle}})^* \Sigma_1 = \Sigma_1 P^* (W_{\mathbf{k}}^{\text{particle}}) (P^*)^{-1} \Sigma_1$, where in the second equality we used Eq. (D1). Thus they have the same Wannier center flow structure.

APPENDIX E: DETAILS ON MEAN-FIELD THEORY AND SYMMETRY ANALYSIS

In this Appendix, we present a detailed mean-field calculation for two models discussed in the main text. Especially, we consider a more general interaction term with Eq. (34) as a special case. The requirement of the form of interaction in order to get a BdG system with PTRS is examined.

1. BKM model

We start from the full Hamiltonian, with a generic repulsive interaction, written in momentum space,

$$\begin{aligned} H & = \sum_{\mathbf{k}} a_{\mathbf{k}}^\dagger h(\mathbf{k}) a_{\mathbf{k}} \\ & + \frac{1}{2M} \sum_{\mathbf{k}, \mathbf{p}, \mathbf{q}, \sigma, \sigma'} U_{\sigma\sigma'} a_{\mathbf{k}+\mathbf{q}, \sigma}^\dagger a_{\mathbf{p}-\mathbf{q}, \sigma'}^\dagger a_{\mathbf{k}, \sigma} a_{\mathbf{p}, \sigma'}, \end{aligned} \quad (\text{E1})$$

where $h(\mathbf{k})$ is given in Eq. (35), M is the total number of unit cells, $U_{\uparrow\uparrow} = U_{\downarrow\downarrow} = U > 0$, $U_{\uparrow\downarrow} = U_{\downarrow\uparrow} = \lambda U$, and $\lambda > 0$ is the interspecies anisotropy. Assuming bosons condense at Γ , the ground-state wave-function ansatz is

$$|\psi\rangle = \frac{1}{\sqrt{\mathcal{N}!}} \left(\sqrt{\mathcal{N}} \sum_{\sigma_s} \psi_{\sigma_s} a_{\Gamma\sigma_s}^\dagger \right)^{\mathcal{N}} |0\rangle,$$

where \mathcal{N} is the total boson number and four complex numbers ψ_{σ_s} satisfy $\sum_{\sigma_s} |\psi_{\sigma_s}|^2 = 1$. Using the following parametrization:

$$(\psi_{A\uparrow}, \psi_{A\downarrow}, \psi_{B\uparrow}, \psi_{B\downarrow}) = (\rho_1 e^{i\phi_1}, \rho_2 e^{i\phi_2}, \rho_3 e^{i\phi_3}, \rho_4 e^{i\phi_4}), \quad (\text{E2})$$

the Gross-Pitaevskii (GP) energy functional density becomes

$$\begin{aligned} \mathcal{E}_{\text{GP}} & = \frac{\langle \psi | H | \psi \rangle}{\mathcal{N}} \\ & = -6t [\cos(\phi_1 - \phi_3) \rho_1 \rho_3 - \cos(\phi_2 - \phi_4) \rho_2 \rho_4] \\ & - \lambda_v (\rho_1^2 + \rho_2^2 - \rho_3^2 - \rho_4^2) \\ & + \frac{nU}{2} - nU (\rho_1^2 + \rho_2^2) (\rho_3^2 + \rho_4^2) \\ & - nU (1 - \lambda) (\rho_1^2 \rho_2^2 + \rho_3^2 \rho_4^2), \end{aligned} \quad (\text{E3})$$

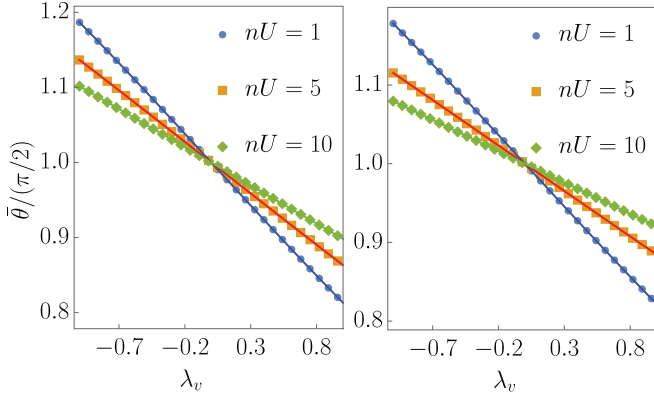


FIG. 7. Mean-field solution of $\theta = 2 \arctan(\rho_3/\rho_1)$ for the BKM model as a function of sublattice imbalance λ_v for interaction anisotropy $\lambda = 0.3$ (left) and $\lambda = 1.5$ (right), obtained by both minimizing Eq. (E3) numerically using the method of simulated annealing (dots) and minimizing Eq. (E4) (left) or Eq. (E5) (right) analytically (solid lines). Note, although $\bar{\theta}$ behaves similarly for $\lambda > 1$ and $\lambda < 1$, they correspond to different ground states, i.e., Z-ferro and XY-ferro, respectively. Other relevant parameters: $\lambda_s/t = 0.06$.

where $n = \mathcal{N}/M$ is the particle number density. Its minimization fixes $\phi_1 = \phi_3$ and $\phi_2 = \phi_4$ [two phases left arbitrary dictated by two U(1) symmetries of the system]. For $\lambda < 1$, we expect the XY-ferro state is favored. By setting $\rho_1 = \rho_2$ and $\rho_3 = \rho_4$, the GP energy functional simplifies to

$$\mathcal{E}_{\text{GP}}|_{\lambda < 1} = -12t\rho_1\rho_3 - 2\lambda_v(\rho_1^2 - \rho_3^2) + \frac{nU}{2}[1 - 4\rho_1^2\rho_3^2 - 2(1 - \lambda)(\rho_1^4 + \rho_3^4)], \quad (\text{E4})$$

with the constraint $\rho_1^2 + \rho_3^2 = 1/2$. Further introducing $(\rho_1, \rho_3) = (1/\sqrt{2})(\cos \frac{\theta}{2}, \sin \frac{\theta}{2})$, then minimizing Eq. (E4) finally fixes $\theta = \bar{\theta}$. For $\lambda > 1$, we expect the Z-ferro state is favored. By setting $\rho_2 = \rho_4 = 0$ (without loss of generality, assuming $\lambda_v > 0$), the GP energy functional simplifies to

$$\mathcal{E}_{\text{GP}}|_{\lambda > 1} = -6t\rho_1\rho_3 + \lambda_v(\rho_3^2 - \rho_1^2) + nU(\frac{1}{2} - \rho_1^2\rho_3^2). \quad (\text{E5})$$

Further introducing $(\rho_1, \rho_3) = (\cos \frac{\theta}{2}, \sin \frac{\theta}{2})$, then minimizing Eq. (E5) finally fixes $\theta = \bar{\theta}$. The above analysis has been confirmed by minimizing Eq. (E3) directly using the method of simulated annealing, as shown in Fig. 7. The mean-field analysis shows that $\bar{\theta}$ decreases (increases) from $\pi/2$ when turning on a positive (negative) sublattice potential λ_v , which physically means that more bosons will condense into the A (B) sublattice. The repulsive interaction suppresses this sublattice imbalance, since it favors a uniform configuration. We note $\bar{\theta}$ is a monotonically decreasing function of λ_v , but never reaches its extreme values, 0 or π , for any finite $|\lambda_v|$.

After obtaining the ground state, we then follow the number-conserving approach [72] to the Bogoliubov theory. Making the substitution

$$a_{\Gamma\sigma s}^{(\dagger)} \rightarrow \left(\mathcal{N} - \sum_{\mathbf{k} \neq \Gamma, \sigma s} a_{\mathbf{k}, \sigma s}^\dagger a_{\mathbf{k}, \sigma s} \right)^{1/2} \psi_{\sigma s}^{(*)},$$

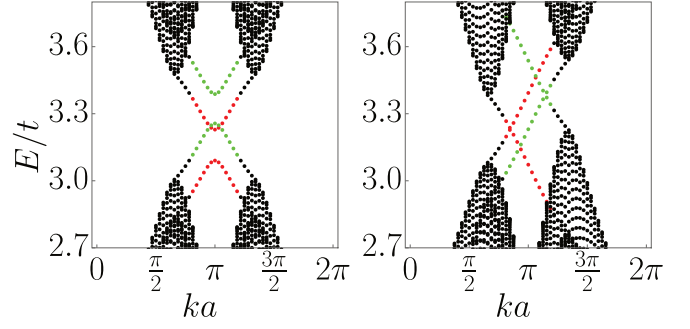


FIG. 8. Bogoliubov excitation spectrum near the middle gap of particle bands for the BKM model in a strip geometry of 64 unit cells (each containing 64 sites) with zigzag edges for $\lambda = 0.3$ (left) and $\lambda = 1.3$ (right). Red (green) points correspond to edge modes, whose wave functions have more than 80% weight on the leftmost (rightmost) unit cell. For both cases, the bosonic Kramers' pair is gone. Other relevant parameters: $nU/t = 1$, $\lambda_s/t = 0.06$, and $\lambda_v/t = 0.1$.

Eq. (E1) can be written, up to the quadratic order in operators, as

$$H_{\text{Bog.}} = \mathcal{N}\mathcal{E}_{\text{GP}} + \sum_{\mathbf{k} \neq \Gamma} a_{\mathbf{k}}^\dagger A_{\mathbf{k}} a_{\mathbf{k}} + (a_{\mathbf{k}}^\dagger B a_{\mathbf{k}}^\dagger + \text{H.c.}), \quad (\text{E6})$$

where

$$A_{\mathbf{k}} = h(\mathbf{k}) - \mu I_4 + h_1, \quad (\text{E7})$$

$$\mu = \sum_{\sigma s, \sigma' s'} \psi_{\sigma s}^* [h(\mathbf{k})]_{\sigma s, \sigma' s'} \psi_{\sigma' s'}, \quad (\text{E8})$$

$$+ n \sum_{\sigma s s'} U_{ss'} \psi_{\sigma s}^* \psi_{\sigma' s'}^* \psi_{\sigma s'} \psi_{\sigma s}, \quad (\text{E9})$$

$$[h_1]_{\sigma s, \sigma' s'} = n \delta_{\sigma, \sigma'} U_{ss'} (\psi_{\sigma s} \psi_{\sigma' s'}^* + \psi_{\sigma' s'}^* \psi_{\sigma s}), \quad (\text{E10})$$

and

$$B_{\sigma s, \sigma' s'} = \frac{n}{2} \delta_{\sigma, \sigma'} U_{ss'} \psi_{\sigma s'} \psi_{\sigma s}. \quad (\text{E11})$$

We plug the mean-field ground-state solution into Eq. (E6), and rewrite it into a BdG form as discussed in Sec. II A. For $1 > \lambda > 0$, the effective Hamiltonian is found to be

$$H_{\mathbf{k}}^{\text{eff}}|_{\lambda < 1} = H_{\mathbf{k}}^{\text{eff}}|_{\lambda = 0} + \frac{\lambda nU}{8} \left\{ i\tau_2 \otimes (\cos \bar{\theta} \Gamma_{13} + \Gamma_{45}) + \tau_3 \otimes \left[\frac{\sin^2 \bar{\theta}}{2} \Gamma_0 + \cos \bar{\theta} (\Gamma_2 + \Gamma_{13}) + \Gamma_{45} \right] \right\}. \quad (\text{E12})$$

For the PTRS operator defined in Eq. (37), the presence of Γ_{13} and Γ_{45} results in a BdG system *without* PTRS for any $1 > \lambda > 0$, while, for $\lambda > 1$, the effective Hamiltonian turns out to be

$$H_{\mathbf{k}}^{\text{eff}}|_{\lambda > 1} = H_{\mathbf{k}}^{\text{eff}}|_{\lambda = 0} + \frac{\lambda nU}{4} \tau_3 \otimes [\Gamma_0 + \cos \bar{\theta} (\Gamma_2 - \Gamma_{15}) - \Gamma_{34}]. \quad (\text{E13})$$

Due to the presence of Γ_{15} and Γ_{34} , the BdG system does *not* possess PTRS either. In Fig. 8, we show the absence of a bosonic Kramers' pair for both $0 < \lambda < 1$ and $\lambda > 1$. In conclusion, the interspecies interactions break the PTRS.

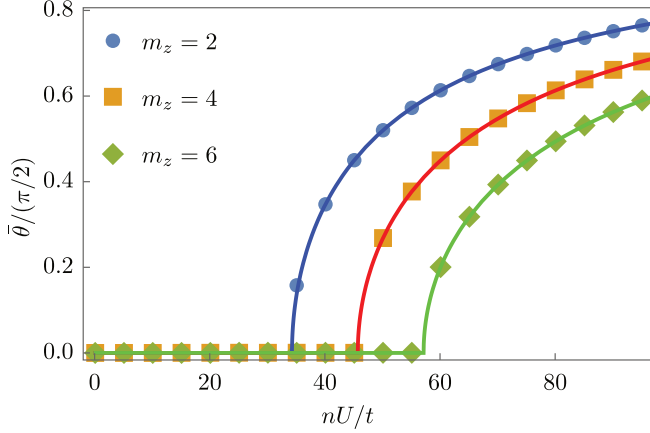


FIG. 9. Mean-field solution of $\theta = 2 \arctan(\rho_2/\rho_1)$ for the BBHZ model as a function of nU for $\lambda = 0.3$, obtained by both minimizing Eq. (E15) numerically using the method of simulated annealing (dots) and minimizing a reduced equation analytically after using the substitution $\rho_1 = \rho_3 = (1/\sqrt{2}) \cos \frac{\theta}{2}$ and $\rho_2 = \rho_4 = (1/\sqrt{2}) \sin \frac{\theta}{2}$ (solid lines). Note for the weakly interacting region, i.e., for U/t small, we always have $\bar{\theta} = 0$.

2. BBHZ model

The full Hamiltonian, with a generic repulsive interaction, in momentum space reads

$$H = \sum_{\mathbf{k}} a_{\mathbf{k}}^{\dagger} h(\mathbf{k}) a_{\mathbf{k}} + \frac{1}{2M} \times \sum_{\mathbf{k}, \mathbf{p}, \mathbf{q}, \eta \eta' s s'} U_{\eta s, \eta' s'} a_{\mathbf{k}+\mathbf{q}, \eta s}^{\dagger} a_{\mathbf{p}-\mathbf{q}, \eta' s'}^{\dagger} a_{\mathbf{k}, \eta' s'} a_{\mathbf{p}, \eta s}, \quad (\text{E14})$$

with $h(\mathbf{k})$ given in Eq. (41), $U_{\eta s, \eta' s'} = U$ if $\eta = \eta'$ and $s = s'$, and $U_{\eta s, \eta' s'} = \lambda U$ otherwise. Physically speaking, we are considering on-site, density-density interaction between all four kinds of bosons (two types \times two pseudospins); this is different from the BKM model, since the latter has two sublattices. Assuming bosons condense at Γ , which is possible for m_z sufficiently large and positive, the ground-state wave-function ansatz is

$$|\psi\rangle = \frac{1}{\sqrt{\mathcal{N}!}} \left(\sqrt{\mathcal{N}} \sum_{\eta s} \psi_{\eta s} a_{\Gamma \eta s}^{\dagger} \right)^{\mathcal{N}} |0\rangle,$$

with four complex numbers satisfying $\sum_s |\psi_{\eta s}|^2 = 1$. Using again the parametrization Eq. (E2), the GP energy functional density then becomes [73]

$$\begin{aligned} \mathcal{E}_{\text{GP}} = & -(4t + m_z)(\rho_1^2 - \rho_2^2 + \rho_3^2 - \rho_4^2) \\ & + nU \left[\frac{1}{2} + (\lambda - 1)(\rho_1^2 \rho_2^2 + \rho_1^2 \rho_3^2 \right. \\ & \left. + \rho_1^2 \rho_4^2 + \rho_2^2 \rho_3^2 + \rho_2^2 \rho_4^2 + \rho_3^2 \rho_4^2) \right]. \quad (\text{E15}) \end{aligned}$$

For $0 \leq \lambda < 1$, Eq. (E15) is minimized by setting $\rho_1 = \rho_3 = (1/\sqrt{2}) \cos \frac{\bar{\theta}}{2}$ and $\rho_2 = \rho_4 = (1/\sqrt{2}) \sin \frac{\bar{\theta}}{2}$ with $\bar{\theta}$ plotted in Fig. 9. Note in the region of the weak-coupling limit, i.e., U/t is small, we always have $\bar{\theta} = 0$, which is assumed to be the case in the following discussion. For $\lambda > 1$, Eq. (E15) is

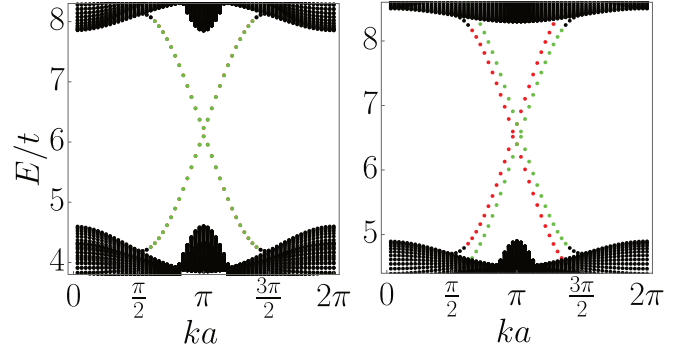


FIG. 10. Bogoliubov excitation spectrum near the middle gap of particle bands for the BBHZ model in a strip geometry of 64 unit cells (each containing 64 sites) for $\lambda = 0.3$ (left) and $\lambda = 1.3$ (right). Red (green) points correspond to edge modes, whose wave functions have more than 80% weight on the leftmost (rightmost) unit cell. Note, for the former case, the left (right) edge modes are completely overlapped due to IS. For both cases, the bosonic Kramer's pair is gone. Other relevant parameters: $nU/t = t_s/t = 1$ and $m_z/t = 2.1$.

simply minimized by setting $\rho_1 = 1$ and $\rho_2 = \rho_3 = \rho_4 = 0$ (or exchange ρ_1 and ρ_3 due to symmetry).

Again, based on the mean-field ground state obtained, we take into account fluctuations by using the Bogoliubov theory. We make the following substitution in Eq. (E14):

$$a_{\Gamma \eta s}^{(\dagger)} \rightarrow \left(\mathcal{N} - \sum_{\mathbf{k} \neq \Gamma, \eta s} a_{\mathbf{k}, \eta s}^{\dagger} a_{\mathbf{k}, \eta s} \right)^{1/2} \psi_{\eta s}^{(*)}.$$

Up to the quadratic order in operators, the Bogoliubov Hamiltonian takes the same form as Eq. (E6), with \mathcal{E}_{GP} given in Eq. (E15) and A, B matrices given by

$$A_{\mathbf{k}} = h(\mathbf{k}) - \mu I_4 + h_1, \quad (\text{E16})$$

$$\mu = \sum_{\eta s, \eta' s'} \psi_{\eta s}^* [h(\mathbf{k})]_{\eta s, \eta' s'} \psi_{\eta' s'} \quad (\text{E17})$$

$$+ n \sum_{\eta s, \eta' s'} U_{\eta s, \eta' s'} \psi_{\eta s}^* \psi_{\eta' s'}^* \psi_{\eta' s'} \psi_{\eta s}, \quad (\text{E18})$$

$$[h_1]_{\eta s, \eta' s'} = nU_{\eta s, \eta' s'} (\psi_{\eta s} \psi_{\eta' s'}^* + \psi_{\eta' s'}^* \psi_{\eta s}), \quad (\text{E19})$$

and

$$B_{\eta s, \eta' s'} = \frac{n}{2} U_{\eta s, \eta' s'} \psi_{\eta' s'} \psi_{\eta s}. \quad (\text{E20})$$

Plugging the mean-field ground-state solution into Eq. (E14), for $1 > \lambda > 0$, the effective Hamiltonian is found to be

$$\begin{aligned} H_{\mathbf{k}}^{\text{eff}}|_{\lambda < 1} = & H_{\mathbf{k}}^{\text{eff}}|_{\lambda = 0} + \frac{\lambda nU}{4} \tau_3 \otimes (-\Gamma_{23} + \Gamma_{45} + 3\Gamma_0 - \Gamma_1) \\ & + \frac{\lambda nU}{4} i\tau_2 \otimes (-\Gamma_{23} + \Gamma_{45}). \quad (\text{E21}) \end{aligned}$$

Noting that, for the PTRS operator defined in Eq. (45), we have [for \mathcal{P} defined in Eq. (46), the plus and minus signs on the RHS are exchanged]

$$\mathcal{T}[\tau_i \otimes \Gamma_{ab}] \mathcal{T}^{-1} = \begin{cases} +\tau_i \otimes \Gamma_{ab} & \text{for } a = 1 \text{ or } b = 1, \\ -\tau_i \otimes \Gamma_{ab} & \text{for } a \neq 1 \text{ and } b \neq 1. \end{cases}$$

Hence the presence of Γ_{23} and Γ_{45} results in a BdG system *without* PTRS (but still IS) for any $1 > \lambda > 0$, while, for $\lambda > 1$, the effective Hamiltonian turns out to be

$$H_{\mathbf{k}}^{\text{eff}}|_{\lambda>1} = H_{\mathbf{k}}^{\text{eff}}|_{\lambda=0} + \frac{\lambda n U}{4} \tau_3 \otimes (-\Gamma_{34} + \Gamma_{25} + 3\Gamma_0 - \Gamma_1). \quad (\text{E22})$$

Again, due to the presence of Γ_{34} and Γ_{25} , the BdG system does *not* possess PTRS either (but still has IS). In Fig. 10, we show the absence of a bosonic Kramers' pair for both $0 < \lambda < 1$ and $\lambda > 1$. In conclusion, the interspecies interactions again break the PTRS.

-
- [1] X.-L. Qi and S.-C. Zhang, Topological insulators and superconductors, *Rev. Mod. Phys.* **83**, 1057 (2011).
- [2] M. Z. Hasan and C. L. Kane, *Colloquium*: Topological insulators, *Rev. Mod. Phys.* **82**, 3045 (2010).
- [3] C.-K. Chiu, J. C. Teo, A. P. Schnyder, and S. Ryu, Classification of topological quantum matter with symmetries, *Rev. Mod. Phys.* **88**, 035005 (2016).
- [4] A. Altland and M. R. Zirnbauer, Nonstandard symmetry classes in mesoscopic normal-superconducting hybrid structures, *Phys. Rev. B* **55**, 1142 (1997).
- [5] M. R. Zirnbauer, Symmetry classes, in *Oxford Handbooks Online*, edited by G. Akemann, J. Baik, and P. Di Francesco, doi: 10.1093/oxfordhb/9780198744191.013.3.
- [6] L. Fu and C. L. Kane, Topological insulators with inversion symmetry, *Phys. Rev. B* **76**, 045302 (2007).
- [7] L. Fu, Topological Crystalline Insulators, *Phys. Rev. Lett.* **106**, 106802 (2011).
- [8] P.-Y. Chang, Topology and entanglement in quench dynamics, *Phys. Rev. B* **97**, 224304 (2018).
- [9] C. Yang, L. Li, and S. Chen, Dynamical topological invariant after a quantum quench, *Phys. Rev. B* **97**, 060304(R) (2018).
- [10] Z. Gong and M. Ueda, Topological Entanglement-Spectrum Crossing in Quench Dynamics, *Phys. Rev. Lett.* **121**, 250601 (2018).
- [11] X. Qiu, T.-S. Deng, G.-C. Guo, and W. Yi, Dynamical topological invariants and reduced rate functions for dynamical quantum phase transitions in two dimensions, *Phys. Rev. A* **98**, 021601(R) (2018).
- [12] H. Shen, B. Zhen, and L. Fu, Topological Band Theory for Non-Hermitian Hamiltonians, *Phys. Rev. Lett.* **120**, 146402 (2018).
- [13] K. Kawabata, K. Shiozaki, and M. Ueda, Anomalous helical edge states in a non-Hermitian Chern insulator, *Phys. Rev. B* **98**, 165148 (2018).
- [14] S. Yao and Z. Wang, Edge States and Topological Invariants of Non-Hermitian Systems, *Phys. Rev. Lett.* **121**, 086803 (2018).
- [15] K. Kawabata, S. Higashikawa, Z. Gong, Y. Ashida, and M. Ueda, Topological unification of time-reversal and particle-hole symmetries in non-Hermitian physics, *Nat. Commun.* **10**, 297 (2019).
- [16] S. Raghu and F. D. M. Haldane, Analogs of quantum-Hall-effect edge states in photonic crystals, *Phys. Rev. A* **78**, 033834 (2008).
- [17] R. Shindou, R. Matsumoto, S. Murakami, and J. I. Ohe, Topological chiral magnonic edge mode in a magnonic crystal, *Phys. Rev. B* **87**, 174427 (2013).
- [18] R. Chisnell, J. S. Helton, D. E. Freedman, D. K. Singh, R. I. Bewley, D. G. Nocera, and Y. S. Lee, Topological Magnon Bands in a Kagome Lattice Ferromagnet, *Phys. Rev. Lett.* **115**, 147201 (2015).
- [19] H. Kondo, Y. Akagi, and H. Katsura, Z_2 topological invariant for magnon spin Hall systems, *Phys. Rev. B* **99**, 041110(R) (2019).
- [20] Z. Wang, Y. D. Chong, J. D. Joannopoulos, and M. Soljačić, Reflection-Free One-Way Edge Modes in a Gyromagnetic Photonic Crystal, *Phys. Rev. Lett.* **100**, 013905 (2008).
- [21] M. C. Rechtsman, J. M. Zeuner, Y. Plotnik, Y. Lumer, D. Podolsky, F. Dreisow, S. Nolte, M. Segev, and A. Szameit, Photonic Floquet topological insulators, *Nature (London)* **496**, 196 (2013).
- [22] V. Peano, M. Houde, C. Brendel, F. Marquardt, and A. A. Clerk, Topological phase transitions and chiral inelastic transport induced by the squeezing of light, *Nat. Commun.* **7**, 10779 (2016).
- [23] R. Fleury, D. L. Sounas, C. F. Sieck, M. R. Haberman, and A. Alu, Sound isolation and giant linear nonreciprocity in a compact acoustic circulator, *Science* **343**, 516 (2014).
- [24] A. H. Safavi-Naeini, J. T. Hill, S. Meenehan, J. Chan, S. Gröblacher, and O. Painter, Two-Dimensional Phononic-Photonic Band Gap Optomechanical Crystal Cavity, *Phys. Rev. Lett.* **112**, 153603 (2014).
- [25] V. Peano, C. Brendel, M. Schmidt, and F. Marquardt, Topological Phases of Sound and Light, *Phys. Rev. X* **5**, 031011 (2015).
- [26] R. Süssstrunk and S. D. Huber, Observation of phononic helical edge states in a mechanical topological insulator, *Science* **349**, 47 (2015).
- [27] S. Furukawa and M. Ueda, Excitation band topology and edge matter waves in Bose-Einstein condensates in optical lattices, *New J. Phys.* **17**, 115014 (2015).
- [28] Z.-F. Xu, L. You, A. Hemmerich, and W. V. Liu, π -Flux Dirac Bosons and Topological Edge Excitations in a Bosonic Chiral p-Wave Superfluid, *Phys. Rev. Lett.* **117**, 085301 (2016).
- [29] M. D. Liberto, A. Hemmerich, and C. Morais Smith, Topological Varma Superfluid in Optical Lattices, *Phys. Rev. Lett.* **117**, 163001 (2016).
- [30] C. L. Kane and E. J. Mele, Z_2 Topological Order and the Quantum Spin Hall Effect, *Phys. Rev. Lett.* **95**, 146802 (2005).
- [31] L. Fu and C. L. Kane, Time reversal polarization and a Z_2 adiabatic spin pump, *Phys. Rev. B* **74**, 195312 (2006).
- [32] R. Yu, X. L. Qi, A. Bernevig, Z. Fang, and X. Dai, Equivalent expression of Z_2 topological invariant for band insulators using the non-Abelian Berry connection, *Phys. Rev. B* **84**, 075119 (2011).
- [33] See, e.g., https://groupprops.subwiki.org/wiki/Symplectic_group for a mathematical definition of symplectic group.
- [34] J. H. P. Colpa, Diagonalization of the quadratic boson Hamiltonian, *Physica A* **93**, 327 (1978).
- [35] J.-P. Blaizot and G. Ripka, *Quantum Theory of Finite Systems* (MIT Press, Cambridge, MA, 1986).
- [36] S. K. Kim and J. L. Birman, Dynamical group $SO(3,2;\mathbb{r})$ of the polariton waves, *Phys. Rev. B* **38**, 4291 (1988).
- [37] W.-M. Zhang, D. H. Feng, and R. Gilmore, Coherent states: Theory and some applications, *Rev. Mod. Phys.* **62**, 867 (1990).
- [38] A. Richaud and V. Penna, Quantum dynamics of bosons in a two-ring ladder: Dynamical algebra, vortexlike excitations, and currents, *Phys. Rev. A* **96**, 013620 (2017).

- [39] V. Peano and H. Schulz-Baldes, Topological edge states for disordered bosonic systems, *J. Math. Phys.* **59**, 031901 (2018).
- [40] C. M. Bender, P. E. Dorey, C. Dunning, A. Fring, D. W. Hook, H. F. Jones, S. Kuzhel, G. Lévai, and R. Tateo, *PT Symmetry* (World Scientific Publishing, 2019).
- [41] M. Lein and K. Sato, Krein-Schrödinger formalism of bosonic Bogoliubov–de Gennes and certain classical systems and their topological classification, *Phys. Rev. B* **100**, 075414 (2019).
- [42] H. Schulz-Baldes and C. Villegas-Blas, Signatures for j -hermitians and j -unitaries on krein spaces with real structures, *Mathematische Nachrichten* **290**, 1840 (2016).
- [43] D. A. Takahashi and M. Nitta, Counting rule of Nambu–Goldstone modes for internal and spacetime symmetries: Bogoliubov theory approach, *Ann. Phys. (NY)* **354**, 101 (2015).
- [44] H. Watanabe, Counting rules of Nambu–Goldstone modes, *Annu. Rev. Condens. Matter Phys.* **11**, 169 (2020).
- [45] J. J. Sakurai, *Modern Quantum Mechanics* (Pearson Education, Harlow, Essex, 2014).
- [46] The proof is similar to the case for the ordinary TRS. Consider
- $$\begin{aligned} \langle\langle\phi, \mathcal{T}\psi\rangle\rangle &= \phi_i^*(\Sigma_3 P)_{ij} \psi_j^* \\ &= \psi_j^*(P^T \Sigma_3)_{ji} \phi_i^* = \langle\langle\psi, \Sigma_3 P^T \Sigma_3 K \phi\rangle\rangle, \end{aligned}$$
- then replacing ϕ by $\mathcal{T}\phi$ and using pseudo-unitarity of P ,
- $$\langle\langle\mathcal{T}\phi, \mathcal{T}\psi\rangle\rangle = \langle\langle\psi, \Sigma_3 P^T \Sigma_3 K P K \phi\rangle\rangle = \langle\langle\psi, \phi\rangle\rangle.$$
- Hence \mathcal{T} is indeed pseudo-antiunitary.
- [47] G. Engelhardt and T. Brandes, Topological Bogoliubov excitations in inversion-symmetric systems of interacting bosons, *Phys. Rev. A* **91**, 053621 (2015).
- [48] R. Resta, What makes an insulator different from a metal? in *Fundamentals Physics of Ferroelectric 2000: Aspen Center for Physics Winter Workshop*, edited by R. E. Cohen and R. A. Mewaldt, AIP Conf. Proc. No. 535 (AIP, Melville, NY, 2000), p. 67.
- [49] S. Kivelson, Wannier functions in one-dimensional disordered systems: Application to fractionally charged solitons, *Phys. Rev. B* **26**, 4269 (1982).
- [50] M. E. Peskin and D. V. Schroeder, *An Introduction To Quantum Field Theory* (Westview Press, New York, 1995).
- [51] F. D. M. Haldane, Model for a Quantum Hall Effect Without Landau Levels: Condensed-Matter Realization of the “Parity Anomaly”, *Phys. Rev. Lett.* **61**, 2015 (1988).
- [52] G. Jotzu, M. Messer, R. Desbuquois, M. Lebrat, T. Uehlinger, D. Greif, and T. Esslinger, Experimental realization of the topological Haldane model with ultracold fermions, *Nature (London)* **515**, 237 (2014).
- [53] T. Fukui and Y. Hatsugai, Quantum spin Hall effect in three dimensional materials: Lattice computation of \mathbb{Z}_2 topological invariants and its application to Bi and Sb, *J. Phys. Soc. Jpn.* **76**, 053702 (2007).
- [54] I. Vasić, A. Petrescu, K. Le Hur, and W. Hofstetter, Chiral bosonic phases on the Haldane honeycomb lattice, *Phys. Rev. B* **91**, 094502 (2015).
- [55] B. A. Bernevig, *Topological Insulators and Topological Superconductors* (Princeton University Press, Princeton, NJ, 2013).
- [56] X.-J. Liu, K. T. Law, and T. K. Ng, Realization of 2D Spin-Orbit Interaction and Exotic Topological Orders in Cold Atoms, *Phys. Rev. Lett.* **112**, 086401 (2014).
- [57] Z. Wu, L. Zhang, W. Sun, X.-T. Xu, B.-Z. Wang, S.-C. Ji, Y. Deng, S. Chen, X.-J. Liu, and J.-W. Pan, Realization of two-dimensional spin-orbit coupling for Bose-Einstein condensates, *Science* **354**, 83 (2016).
- [58] W. Sun, B.-Z. Wang, X.-T. Xu, C.-R. Yi, L. Zhang, Z. Wu, Y. Deng, X.-J. Liu, S. Chen, and J.-W. Pan, Highly Controllable and Robust 2D Spin-Orbit Coupling for Quantum Gases, *Phys. Rev. Lett.* **121**, 150401 (2018).
- [59] J. K. Asbóth, L. Oroszlány, and A. Pályi, *A Short Course on Topological Insulators* (Springer International Publishing, Berlin, 2016).
- [60] B. A. Bernevig, T. L. Hughes, and S.-C. Zhang, Quantum spin Hall effect and topological phase transition in HgTe quantum wells, *Science* **314**, 1757 (2006).
- [61] L.-J. Lang, S.-L. Zhang, and Q. Zhou, Nodal Brillouin-zone boundary from folding a Chern insulator, *Phys. Rev. A* **95**, 053615 (2017).
- [62] J. Li, R.-L. Chu, J. K. Jain, and S.-Q. Shen, Topological Anderson Insulator, *Phys. Rev. Lett.* **102**, 136806 (2009).
- [63] N. Goldman, J. Beugnon, and F. Gerbier, Detecting Chiral Edge States in the Hofstadter Optical Lattice, *Phys. Rev. Lett.* **108**, 255303 (2012).
- [64] N. Goldman, J. Dalibard, A. Dauphin, F. Gerbier, M. Lewenstein, P. Zoller, and I. B. Spielman, Direct imaging of topological edge states in cold-atom systems, *Proc. Natl. Acad. Sci. U.S.A.* **110**, 6736 (2013).
- [65] N. Goldman, J. Beugnon, and F. Gerbier, Identifying topological edge states in 2d optical lattices using light scattering, *Eur. Phys. J.: Spec. Top.* **217**, 135 (2013).
- [66] A. Celi and L. Tarruell, Probing the edge with cold atoms, *Science* **349**, 1450 (2015).
- [67] P. T. Ernst, S. Götze, J. S. Krauser, K. Pyka, D.-S. Lühmann, D. Pfannkuche, and K. Sengstock, Probing superfluids in optical lattices by momentum-resolved Bragg spectroscopy, *Nat. Phys.* **6**, 56 (2009).
- [68] L. Fu, C. L. Kane, and E. J. Mele, Topological Insulators in Three Dimensions, *Phys. Rev. Lett.* **98**, 106803 (2007).
- [69] H. Kondo, Y. Akagi, and H. Katsura, Three-dimensional topological magnon systems, *Phys. Rev. B* **100**, 144401 (2019).
- [70] Y. Ando and L. Fu, Topological crystalline insulators and topological superconductors: From concepts to materials, *Annu. Rev. Condens. Matter Phys.* **6**, 361 (2015).
- [71] Y.-J. Wu, W.-Y. Zhou, and S.-P. Kou, Bogoliubov excitations in the Bose-Hubbard extension of a Weyl semimetal, *Phys. Rev. A* **95**, 023620 (2017).
- [72] Y. Kawaguchi and M. Ueda, Spinor Bose–Einstein condensates, *Phys. Rep.* **520**, 253 (2012).
- [73] The GP energy functional is independent of all phase factors ϕ_i , $i = 1, \dots, 4$, due to the existence of both two exact $U(1)$ symmetries and accidental symmetries at mean field level. The latter can be lifted by considering quantum fluctuations, e.g., Ref. [74].
- [74] Y.-Z. You, Z. Chen, X.-Q. Sun, and H. Zhai, Superfluidity of Bosons in Kagome Lattices with Frustration, *Phys. Rev. Lett.* **109**, 265302 (2012).